Chapter HG (Hydrocarbon Potential of Brookian Strata)

MODELING OIL GENERATION IN THE UNDEFORMED PART OF THE ARCTIC NATIONAL WILDLIFE REFUGE 1002 AREA

by David W. Houseknecht[1] and Daniel O. Hayba[2]

in The Oil and Gas Resource Potential of the 1002 Area, Arctic National Wildlife Refuge, Alaska, by ANWR Assessment Team, U.S. Geological Survey Open-File Report 98-34.

1998

[1] U.S. Geological Survey, MS 915, Reston, VA 20192
[2] U.S. Geological Survey, MS 956, Reston, VA 20192

TABLE OF CONTENTS

FIGURES

Click here or on this symbol in the toolbar to return.

TABLE

Click here or on this symbol in the toolbar to return.

ABSTRACT

Burial, thermal, and oil-generation histories for the undeformed part of the ANWR 1002 area were modeled using a geologic framework established with seismic stratigraphy. Modeling was conducted at fifty geographically distributed points by generating synthetic well data from the seismic stratigraphic framework. Data from exploration wells located west of the ANWR 1002 area helped to constrain ages and lithologies of stratigraphic units, as well as heat flow and thermal maturity parameters. Attempts to establish thermal parameters that satisfy all constraining data yielded incongruent results, so model heat flow was adjusted to achieve a match between calculated and measured (empirical) vitrinite reflectance profiles.

Model results suggest that at the base of the Brookian section vitrinite reflectance values fall within the oil window across most of the study area. Based on kinetics of type II kerogen, calculated transformation ratios at the base of the Brookian section range from ~0.2 to ~1.0, indicating that the overlying Brookian section throughout most of the undeformed part of the ANWR 1002 area is oil prospective. Modeling the timing of the main phase of oil generation suggests that the Mikkelsen high represents a focus of relatively recent oil generation and that the age of oil generation increases southward, eastward, and northward away from the Mikkelsen high. The age of the main phase of oil generation at the base of the Brookian section ranges from ~40 Ma along the trend of the Marsh Creek anticline to 0 Ma near the crest of the Mikkelsen high. These results suggest that the timing for oil generation, reservoir deposition, and trap formation is favorable, even for the youngest potential reservoirs and traps identified in this assessment.

INTRODUCTION

An important aspect of assessing the hydrocarbon potential of the Arctic National Wildlife Refuge (ANWR) 1002 area is estimating the timing of oil generation relative to the deposition of potential reservoirs and the development of traps, and estimating the thermal preservation of any oil generated. In recent years, an emphasis of petroleum research has been the integration of burial history, thermal history, and kinetics of hydrocarbon generation to model these chemical reactions.

The objective of this paper is to model oil generation in the undeformed part of the ANWR 1002 area so that estimates can be made regarding the timing

of oil generation, the degree to which the chemical transformation of kerogen to hydrocarbons has proceeded, and the likely preservation state of oil considering inferred thermal history. Oil generation is the focus of this paper because crude oil determines the economic viability of petroleum resources on the North Slope.

PROCEDURES

The modeling involves integration of (1) burial history inferred from Brookian seismic stratigraphy in the undeformed part of the 1002 area, (2) thermal history inferred from temperature and thermal maturity data from wells located adjacent to the 1002 area, and (3) hydrocarbon generation kinetic data representative of kerogen present in basal Brookian strata.

We infer burial history of the undeformed part of the 1002 area from the seismic stratigraphy of Brookian strata described by Houseknecht and Schenk (Chap. BS). As described there, the seismic grid used in this study permits ties to several key wells adjacent to the ANWR 1002 area, and permits ties to outcrop sections within and outside the ANWR 1002 area. The ages and lithologies of Brookian depositional sequences are constrained by data from wells and outcrops correlated to seismic data, as well as from seismic expression of the depositional sequences.

Once depositional sequences were defined and mapped throughout the undeformed part of the 1002 area, fifty "synthetic wells" were generated from the seismic interpretations to produce a grid of burial history control points more-or-less equally distributed across the study area (Fig. HG1). Several of the synthetic wells are located outside the ANWR 1002 area and close to well control so that correlations between actual well data and synthetic well data could be established. Inferred stratigraphic data for each synthetic well, including age, lithology, and thickness of each depositional sequence, were imported into a modeling program (BasinMod version 5.41) and used to construct a burial history for each of the fifty locations.

The initial step in modeling the thermal history of the study area involved the use of bottom-hole temperature data (Nelson and others, Chap. WL) from wells west of the Canning River to estimate heat flow. Bottom-hole temperature data were corrected for circulation time. We applied default values for thermal conductivity calculated as a function of lithology and burial depth to estimate current heat flow using two approaches because of the

presence of permafrost. The first approach considers the base of permafrost as a datum, assumes a temperature of -1°C at that datum, and adjusts the depths of bottom hole temperature measurements relative to that datum. The second approach considers the present land surface as a datum, assumes a surface temperature of -8.5°C (representative temperature at top of permafrost; Lachenbruch and Marshall, 1986; Brewer, 1987), and uses depths of bottom-hole temperature measurements relative to the datum.

Applying these estimates for the present heat flux through geologic time, we calculated depth vs. vitrinite reflectance profiles using a kinetic model (Burnham and Sweeney, 1989; Sweeney and Burnham, 1990). Default thermal conductivities included in the modeling application were applied to mixes of sandstone, siltstone, and shale estimated for each depositional sequence from well logs and seismic expression. The calculated depth vs. vitrinite reflectance trend then was compared to measured depth vs. vitrinite reflectance profiles from wells. If a reasonable fit between model results and measured results was not achieved, heat flow, thermal conductivity, and certain burial history parameters (e.g., amount of missing section at erosional surfaces) were varied until a suitable match was achieved between modeled and measured depth vs. vitrinite reflectance profiles. This approach has become widely accepted in recent years and is similar to that described by Waples (1994). Published values of heat flow and thermal conductivity provided a basis for evaluating whether the results are geologically reasonable. Heat flow values for a broad range of geologic settings have been compiled by Gretener (1981), and thermal conductivity values for a variety of lithologies have been compiled by Blackwell and Steele (1989). Heat flow and thermal conductivity estimates for the western Alaska North Slope have been reported by Deming and others (1992). Thermal history constraints thus established using well control were projected into the ANWR 1002 area and applied to the burial histories of synthetic wells within the 1002 area.

Throughout the undeformed part of the ANWR 1002 area, a major break in the stratigraphic section occurs where either Cretaceous or Tertiary strata rest unconformably on Paleozoic rocks. The former is the Lower Cretaceous Unconformity (LCU) and the latter has been termed the basal Tertiary unconformity (BTU) (Bird, Chap. GG; Houseknecht and Schenk, Chap. BS). This boundary displays persistent and distinct seismic expression and represents a fundamental seismic mapping horizon. We use that horizon as the approximate base of the Brookian section for modeling purposes, although in so doing we include a few hundred feet of strata that are not

formally part of the Brookian "sequence" (including the Kemik Sandstone and Pebble shale unit; Bird and Molenaar, 1987; Bird, Chap. GG).

The best known oil-prone source rock in the Brookian stratigraphic section is the Hue Shale, particularly the lower 150 to 300 feet which includes the "highly radioactive zone" (HRZ) (Magoon and others, 1987; Anders and others, 1987; Lillis and others, Chap. OA; Keller and Bird, Chap. SR; Magoon and others, Chap. PS). However, the continuity of the Hue Shale across the entire study area is not certain and there is geochemical evidence that oil has been generated from younger source rocks that have not been identified (Houseknecht and Schenk, Chap. BS; Magoon and others, Chap. PS). For these reasons, our modeling has focused on the time and temperature histories of depositional sequences that may contain source rocks, and has not focused on specific source rock intervals such as the HRZ.

A series of maps was constructed to illustrate the spatial distribution of the following parameters at the LCU/BTU (i.e., approximate base of the Brookian stratigraphic section): (1) vitrinite reflectance, (2) transformation ratio of type II kerogen, (3) age for onset of the main phase of oil generation, and (4) age for end of the main phase of oil generation. Type II kerogen kinetics were used in this modeling to estimate oil generation parameters because they closely match hydrocarbon generation kinetics of the kerogen found in the Hue Shale, as determined experimentally (Lillis and others, Chap. OA).

ESTABLISHING MODELING CONSTRAINTS USING WELL DATA

Ages and lithologies of the seismic sequences mapped throughout the study area were constrained using wells in the Point Thomson area, along with the E De K Leffingwell, Alaska State J-1, and Beli Unit 1 wells (Fig. HG1). Bottom-hole temperature and vitrinite reflectance data from those wells helped establish thermal constraints for modeling. The following sections summarize the results of our attempts to constrain thermal modeling parameters using well data.

Depth - Vitrinite Reflectance Data

This study relies on vitrinite reflectance data from wells located near the ANWR 1002 area as a key modeling constraint. Most of the data has been

released to the public domain by industry and there is little information available regarding data collection. It is likely the data set contains scatter arising from variation among analysts and techniques, but we have no way of evaluating the accuracy or precision of the data. Nevertheless, we use the data to define general depth - vitrinite reflectance gradients and spatial trends in thermal maturity. Additional information and analysis of this vitrinite reflectance data set are provided by Bird and others (Chap. VR).

An interpretation problem is encountered in the depth - vitrinite reflectance profiles from wells in the Point Thomson area. At depths greater than about 7500 feet, data from those wells define a relatively orderly increase in vitrinite reflectance with depth as would be expected. However, at shallower depths the data define a trend of approximately constant vitrinite reflectance and display significant scatter; individual mean values for samples in this shallow zone are mostly in the range of 0.4 to 0.5 percent vitrinite reflectance. Figs. HG2 through HG6 illustrate these trends in the vitrinite reflectance profiles. This shallow trend of nearly uniform vitrinite reflectance cannot be explained as the result of caving, as the reflectance values are too high and show no relationship to casing points (Figs. HG2 - HG6). We infer that these data represent a predominance of recycled vitrinite among the measured population, and that only the deeper vitrinite reflectance gradient is indicative of the thermal maturation history of the Point Thomson area. Depth - vitrinite reflectance profiles displaying some characteristics similar to these have been interpreted to be the result of the influence of geopressure on heat transport (e.g., Law and others, 1989). However, geopressures are observed only in the deep, shale-rich part of the Brookian section and modeling results suggest that most of the shallow stratigraphic interval has not been geopressured in the past. For these reasons, this possiblility is not considered a likely explanation for the observed vitrinite reflectance profiles.

The recycled vitrinite interpretation is consistent with burial history estimates for the Point Thomson area. The vitrinite reflectance values observed at shallow depths (0.4 to 0.5%) would have required a burial depth of at least 5,000 to 7,000 feet based on results of modeling presented in subsequent sections. These depths of burial are unrealistic considering the seismic stratigraphic analysis (Houseknecht and Schenk, Chap. BS). Apatite fission track evidence also suggests that strata in the Point Thomson area currently are near maximum temperature (O'Sullivan and others, 1993).

Data from the E De K Leffingwell well also are difficult to interpret in this context because the entire depth - vitrinite reflectance dataset displays an extremely low gradient throughout the Brookian section (Fig. HG7). Data down to 5,000 feet or deeper can be interpreted to display the influence of recycled vitrinite, but that interpretation is equivocal (Fig. HG7).

Data from two wells farther south (Alaska State J-1 and Beli Unit 1) either do not display shallow intervals of uniform vitrinite reflectance values or display them at depths of less than 5000 feet (Figs. HG8 and HG9). This observation may indicate that no significant volume of recycled vitrinite is present, that vitrinite reflectance measurements from recycled vitrinite exert a minor influence on the overall dataset, or that an interval of uniform reflectance representing recycled vitrinite has been thinned by erosion. The latter interpretation is consistent with the erosional truncation of Brookian depositional sequences in the vicinity of these wells (Houseknecht and Schenk, Chap. BS).

An additional line of evidence may support the interpretation that the presence of recycled vitrinite results in approximately uniform reflectance measurements in the upper part of the Brookian section. A compilation of vitrinite reflectance measurements from outcrops and from seismic shotholes throughout the ANWR 1002 area shows that the thermal maturity from surface and near-surface samples is remarkably uniform over a large part of the 1002 area, ranging between 0.3 and 0.5 percent vitrinite reflectance (Bird and others, Chap. VR, Plate VR1). This uniformity belies the fact that Brookian strata from which these samples were collected range in age from Eocene to Miocene and that the amount of section eroded from the sample locations likely ranges from a few hundred to several thousand feet. The presence of a voluminous population of recycled vitrinite could explain this plateau of vitrinite reflectance values.

Based on the interpretation presented above, we focused on the depth - vitrinite reflectance gradients in the lower part of the Brookian section as a basic constraint for thermal history modeling and did not attempt to adjust our models to produce calculated vitrinite reflectance values to match those observed in the shallow parts of the wells.

Water Depth

Considering the range of water depths inferred for Brookian depositional systems (Houseknecht and Schenk, Chap. BS), we attempted to incorporate temporal variations in water depth into the modeling. Water depth through Brookian time was estimated from interpretations of depositional systems represented by each of the Brookian depositional sequences. For the Point Thomson area, inferred water depth increases from zero at the end of LCU development to a maximum of 1500 feet during accumulation of late Cretaceous turbidites (sequence F of Houseknecht and Schenk, Chap. BS). Progressive shallowing to near zero is inferred to have occurred during progradation of Paleocene to early Eocene slope, shelf, and non-marine depositional systems represented by sequences E and D (Houseknecht and Schenk, Chap. BS). Water deepened abruptly to perhaps 500 feet and then shallowed to ~250 feet during the Eocene (sequence C of Houseknecht and Schenk, Chap. BS) and average water depth likely was relatively stable (shallow shelf; ~250 feet) during much of the Oligocene and Miocene (sequences B and A, respectively, of Houseknecht and Schenk, Chap. BS). Water depth is inferred to have shallowed to zero at approximately 5 Ma, when the unconformity developed between Miocene and Pliocene-Pleistocene strata. The temporal trend in water depth is illustrated in the geohistory diagrams presented later in this chapter.

We applied this inferred bathymetric history to most burial models, despite the likelihood that water depth varied across the study area as the result of retrogradational and progradational sedimentation. The main exception to the general model is that the latest shallowing to zero depth is assumed to occur earlier for locations south of Point Thomson. This assumption is based on the inference that uplift and erosion of Brookian strata started approximately 25 Ma along the Marsh Creek anticline (O'Sullivan and others, 1993) and migrated northward through time.

Surface Temperature

Surface temperature similarly was varied through time based on inferred paleoclimate reconstructions (Habicht, 1979; Parrish and Barron, 1986). Our models assume the following surface temperatures: 10°C at 130 Ma, 5°C at

45 Ma, 0°C at 10 Ma, -5°C at 2 Ma, and -8.5°C at 0 Ma. In addition, adjustments were made to surface temperatures to account for the effect of water depth, using the general guidelines suggested by Waples (1994, reporting a personal communication from Yukler).

Heat Flow Estimates

Point Thomson Area. Data from eight wells in the Point Thomson area were used in the analysis. Bottom hole temperature data are available from Alaska State C-1, Point Thomson Unit 1, Point Thomson Unit 2, West Staines (18-9-23), and West Staines State 2 (Fig. HG1). Vitrinite reflectance data are available from Point Thomson Unit 1, Point Thomson Unit 3, Alaska State D-1, Alaska State F-1, and West Staines State 2 (Figs. HG2 to 6).

Using the first approach for estimating heat flow (datum = base of permafrost), estimates for individual wells range from 46 to 50 mW/m^2 (Table HG1). Combining all bottom-hole temperature data from the five wells for which data are available into a composite results in a calculated heat flow of 48 mW/m^2. Application of this heat flow to the entire Brookian burial history yields a calculated depth vs. vitrinite reflectance gradient substantially higher than measured, with calculated values lower than measured at shallow depths and higher than measured in the lower part of the Brookian section.

Using the second approach (datum = ground surface), estimates of heat flow from individual wells range from 38 to 46 mW/m^2 (Table HG1) and the result from a composite is 43 mW/m^2. Application of this heat flow to the entire Brookian burial history yields a calculated depth vs. vitrinite reflectance gradient that is somewhat higher than that of the measured trend (but a closer fit than results of the first approach), with calculated values lower than measured at shallow depths and higher than measured in the lower part of the Brookian section.

Near E De K Leffingwell Well. The first approach for estimating heat flow (datum = base of permafrost) yields a value of 45 mW/m^2. Application of this heat flow to the entire Brookian burial history yields a calculated depth vs. vitrinite reflectance gradient much higher than measured, with calculated vitrinite reflectance similar to measured values at shallow depths and much higher than measured in the lower part of the Brookian section.

The second approach (datum = ground surface) yields a heat flow estimate of 33 mW/m^2. Application of this heat flow to the entire Brookian burial history yields a calculated depth vs. vitrinite reflectance gradient higher than measured (but a closer fit than results of the first approach), with calculated values lower than measured at shallow depths and higher than measured in the lower part of the Brookian section.

Near Alaska State J-1 Well. The first approach for estimating heat flow (datum = base of permafrost) yields a value of 55 mW/m^2. Application of this heat flow to the entire Brookian burial history yields a calculated depth vs. vitrinite reflectance gradient much higher than measured, with calculated vitrinite reflectance similar to measured values at shallow depths and much higher than measured in the lower part of the Brookian section.

The second approach (datum = ground surface) yields a heat flow estimate of 37 mW/m^2. Application of this heat flow to the entire Brookian burial history yields a calculated depth vs. vitrinite reflectance gradient higher than measured (but a closer fit than results of the first approach), with calculated values lower than measured at shallow depths and higher than measured in the lower part of the Brookian section.

Near Beli Unit 1 Well. The first approach for estimating heat flow (datum = base of permafrost) yields a value of 55 mW/m^2. Application of this heat flow to the entire Brookian burial history yields a calculated depth vs. vitrinite reflectance gradient higher than measured, with calculated vitrinite reflectance significantly higher than measured values throughout the Brookian section.

The second approach (datum = ground surface) yields a heat flow estimate of 50 mW/m^2. Application of this heat flow to the entire Brookian burial history yields a calculated depth vs. vitrinite reflectance gradient close to, but slightly higher than, measured. However, calculated vitrinite reflectance values are significantly higher than measured throughout the Brookian section.

Discussion of Modeling Parameters

The results reported in the preceding paragraphs do not produce satisfactory inputs for modeling the thermal history of the Brookian section within the ANWR 1002 area for two reasons. (1) Calculated heat flow values are lower than typically reported for similar geologic settings. Worldwide “average”

heat flow values commonly are cited to be around 60 to 65 mW/m^2 (Gretener, 1981). In a nearby example, Deming and others (1992) reported twenty estimates of "deep heat flow" from the western Alaska North Slope that range from 44 to 93 mW/m^2. In the case of our first approach (datum = base of permafrost) the range of heat flow we calculated (45 to 55 mW/m^2) overlaps with only two of the twenty estimates reported by Deming and others (1992) and the results of our second approach (33 to 50 mW/m^2) overlap even less. On the other hand, a contour map of deep heat flow presented by Deming and others (1992) illustrates a trend of decreasing heat flow eastward. The 40 and 50 mW/m^2 contours of Deming and others (1992) project northeastward from the National Petroleum Reserve - Alaska in a pattern that would intersect the coastline between Prudhoe Bay and Point Thomson (see Fig. 6b of Deming and others, 1992), suggesting that the estimated heat flow values we reported above may be reasonable.

(2) Application of calculated heat flow values to the entire burial history of the Brookian section results in calculated depth vs. vitrinite reflectance gradients that are poor matches to empirical data. In all cases, measured depth - vitrinite reflectance profiles display significantly lower gradients than those calculated by applying estimates of present heat flow to the entire burial history. This observation suggests that temporal variation in the overall thermal regime exerted a significant influence on thermal maturation of the Brookian section, and several specific processes may have played a role. (a) Heat flow may have changed through time as the result of evolving tectonic processes. (b) Geopressured sediment may have acted as a thermal insulator during certain intervals of the burial history, thereby reducing the effective thermal conductivity of the Brookian section. (c) Advective fluid flow may have perturbed the "normal" conductive heat flow regime by transporting heat vertically and laterally through the Brookian section. Advection may have been driven by tectonic elevation of the Brooks Range, geopressure related to compaction disequilibrium, geopressure related to hydrocarbon generation, and/or pressure induced by advancing thrust sheets.

In an attempt to find a satisfactory solution to this problem, we experimented by varying both heat flow and thermal conductivity of Brookian depositional sequences through time. Although we were able to match both depth - temperature and depth - vitrinite reflectance profiles using this approach, the time dependent variance of input parameters was too arbitrary (i.e., not related to observable geologic conditions such as depth to basement or proximity to thrust front) to use with confidence in the absence of well data (i.e., within the

ANWR 1002 area). For this reason, we chose to apply a reduced heat flow, held constant throughout the Brookian burial history, that results in a good match to the measured depth - vitrinite reflectance profiles. This solution involves the application of heat flow values that are substantially lower than typically observed in similar geologic settings and results in current depth - temperature profiles that are lower than observed. Nevertheless, we believe this is the least arbitrary approach to matching depth - vitrinite reflectance profiles and to estimating the timing of oil generation.

Heat flow values used in modeling are shown in Table HG1. For synthetic wells within the ANWR 1002 area, heat flow values used in modeling were graduated from north (highest values) to south (lowest values). Note that this approach results in the use of heat flow values somewhat higher than certain nearby well control (i.e., E De K Leffingwell and Alaska State J-1 wells). We opted for this approach because of the comparatively low heat flow values obtained from analysis of bottom-hole temperature data from those two wells.

Because of the reservations enumerated above, we have initiated thermal modeling that incorporates heat transport by advective fluid flow. The initial results of that effort are reported by Hayba and others (Chap. FF). We anticipate that continued efforts will refine our view of the thermal history of the ANWR 1002 area.

RESULTS OF BURIAL HISTORY AND OIL GENERATION MODELING

Point Thomson Area

Brookian geohistory (burial and bathymetric history) in the Point Thomson area is illustrated in Fig. HG10. The burial history is characterized by low sediment accumulation rates during the Cretaceous (sequences F and G of Houseknecht and Schenk, Chap. BS), and rapid sediment accumulation rates during the Tertiary.

Fig. HG11 illustrates measured and calculated depth - vitrinite reflectance profiles for the Point Thomson area. A heat flow value of 42.5 mW/m^2 was used to achieve a reasonable match between measured data inferred to represent the indigenous profile and the calculated profile. The resultant plot

of calculated vitrinite reflectance projects to a value between 0.7 and 0.8 percent at the LCU, which is close to measured values.

This heat flow was applied to the entire Brookian burial history to estimate degree and timing of oil generation. Assuming that the kerogen in sequences F and G (which include the Hue Shale) can be represented by type II kerogen kinetics (Burnham and Sweeney, 1989; Sweeney and Burnham, 1990), this model indicates that the kerogen transformation ratio at the base of the Brookian section is about 0.3 (i.e., kerogen to hydrocarbon transformation process is ~30% complete), the base of the section entered the main phase of oil generation (defined as transformation ratio of 0.25) about seven million years ago, and that the end of the main phase of oil generation has not yet been reached (Fig. HG12).

As shown in Fig. HG10, this model suggests that the lower part of sequences F and G barely have entered the "oil window" and that the remainder of the Brookian section has not yet entered the oil window.

ANWR 1002 Area

The approach illustrated in the preceding section was applied to all fifty synthetic wells in the study area and a series of maps was prepared to summarize key results. Because the total thickness of the Brookian section has exerted an important influence on thermal maturation, a generalized total Brookian isopach map is provided in Fig. HG13. This map represents the sum total of the Brookian sequence isopach maps presented by Houseknecht and Schenk (Chap. BS).

Fig. HG14 is an illustration of Brookian geohistory within part of the ANWR 1002 area that contains a Brookian section more than 20,000 feet thick (Fig. HG13). Although the overall pattern of sediment accumulation is similar to that illustrated in Fig. HG10, a few important differences exist. First, the combined sequence F and G is absent owing to either erosion or slumping induced by slope failure during the Paleocene (Houseknecht and Schenk, Chap. BS). Second, sequence D is absent, apparently due to erosion during the Eocene. Third, the total Brookian section is considerably thicker than in the Point Thomson area.

The depth - vitrinite reflectance profile calculated for the geohistory discussed above is illustrated in Fig. HG15. The calculated profile projects to a value of

approximately 1.3 percent at the base of the Brookian section, suggesting that oil generation and expulsion are complete and any remaining oil in this part of the section is undergoing thermal cracking to lighter hydrocarbons.

For the purpose of modeling the timing of oil generation at this location, we assumed that sequence E contains type II kerogen and that sequence C contains type III kerogen. The presence of type II kerogen in sequence E is hypothesized based on seismic stratigraphic observations (Houseknecht and Schenk, Chap. BS), but this cannot be confirmed because no samples are available. The assumption of type III kerogen in sequence C is reasonable in light of many analyses from the Canning Formation (Magoon and others, Chap. PS). As illustrated in Fig. HG14, our model suggests that the main phase of oil generation in sequence E occurred at shallower depths and ended about 12 Ma, and that late generation is nearing completion. In contrast, the basal part of sequence C appears to be just entering the main phase of oil generation at a relatively deeper depth (Fig. HG14). These differences are primarily due to the kinetic differences between type II and type III kerogen.

The relative timing of oil generation is shown in Fig. HG16. The base of sequence E passed rapidly through the main phase of oil generation between ~42 and ~37 Ma, as indicated by the red line (Fig. HG16), corresponding to an interval of rapid sediment accumulation within sequence C. The top of sequence E passed less quickly through the main phase of oil generation between ~27 and ~12 Ma, as indicated by the blue line (Fig. HG16). In contrast, the base of sequence C is just at the threshold of the main phase of oil generation (Fig. HG16).

Thermal Maturity. Vitrinite reflectance is used widely as an index of thermal maturity, and a map of calculated vitrinite reflectance at the base of the Brookian section (i.e., at the LCU or BTU) provides a useful basis for considering thermal maturity of Brookian strata within the ANWR 1002 area (Fig. HG17). That map suggests that vitrinite reflectance at the base of the Brookian section increases from 0.7 - 0.8% along the western 1002 boundary to 0.8 - 0.9% over a broad area north of the Marsh Creek anticline and west of the "Hulahula low." There appears to be an abrupt increase in vitrinite reflectance into the Hulahula low, corresponding to an increase in thickness of the Brookian section to more than 20,000 feet, and maximum calculated values of more than 1.4% vitrinite reflectance occur near the coastline in the Hulahula low (Fig. HG17).

The pattern of vitrinite reflectance illustrated in Fig. HG17 appears to have both north-south and west-east oriented elements. The north-south trending iso-reflectance contours are most evident in the least deformed areas north of the Marsh Creek anticline and appear to parallel the total Brookian isopach contours (Fig. HG13); they seem to reflect the predominant influence of stratigraphic burial throughout Tertiary time. The west-east trending iso-reflectance contours are most evident along the deformation front (i.e., Marsh Creek anticline) and appear to parallel structural strike. Although it is tempting to interpret a structural control, the burial histories from which the vitrinite reflectance values were calculated are based on sequence stratigraphy only and do not include thrust burial. However, this pattern also is parallel to isopachs of Paleocene and Eocene depositional sequences presented by Houseknecht and Schenk (Chap. BS). It is likely that the west-east iso-reflectance contours reflect the primary influence of Paleocene and Eocene stratigraphic burial, which increases to the south and southeast.

Based on Fig. HG17, it can be inferred that source rocks near the base of the Brookian section have reached levels of thermal maturity indicating that oil generation is mostly or totally complete across the entire study area. In the "Hulahula low" the base of the Brookian section has reached levels of thermal maturity at which oil is thermally cracked to lighter hydrocarbons (i.e., the main gas generation window; Fig. HG15). Above the modeled horizon, most of the Brookian stratigraphic section is characterized by levels of thermal maturity within or below the "oil window" throughout the study area (Figs. HG 11 and HG15), indicating favorable preservation potential for any oil that migrated into this section from source rocks deeper in the section.

Transformation Ratio. A measure of the degree to which kerogen has been transformed to hydrocarbon is transformation ratio, which is based on the kinetics of the transformation process. Fig. HG18 is a map of transformation ratio at the base of the Brookian section, calculated using type II kerogen kinetics. Although this map generally is similar to the vitrinite reflectance map of Fig. HG19, it likely provides a more realistic perspective of the degree to which oil-prone kerogen near the base of the Brookian section has been transformed to hydrocarbons because the kinetics of the two chemical reactions (i.e., vitrinite maturation and hydrocarbon generation from type II kerogen) are different.

The map of transformation ratio suggests that the kerogen-to-hydrocarbon transformation is about 25 percent complete from the Point Thomson area

southward toward the Beli Unit 1 well. The transformation ratio increases to >0.5 just inside the ANWR 1002 area, and increases to >0.7 farther east. The contours representing transformation ratios of 0.25, 0.50, and 0.75 generally are oriented north-south, although they display much subtle detail related to local geology. For example, all three contour lines are bowed to the east around the Mikkelsen high, extending from the Point Thomson area eastward towards Camden Bay (Fig. HG18). A 1.0 transformation ratio contour trends diagonally across the 1002 area, approximately coincident with the structural front defined by the Marsh Creek anticline (Fig. HG18). This transformation ratio approximates the area where it would be expected that type II kerogen-to-hydrocarbon reaction would have reached completion and no additional potential exists for oil generation. We reiterate that the map of transformation ratio is calculated for the base of the Brookian section and that overlying strata would be characterized by lower transformation ratios.

The map of estimated transformation ratios (Fig. HG18) indicates that the type II kerogen-to-hydrocarbon reaction is mostly to entirely complete across most of the study area, suggesting that oil generation and expulsion from source rocks near the base of the Brookian section are essentially complete. It also can be inferred that strata located up-dip or up-section from the modeled horizon are in favorable positions to have been charged with oil generated from source rocks near the base of the Brookian section.

Timing of Hydrocarbon Generation. The onset of the main phase of oil generation commonly is defined as a transformation ratio of 0.25. The age at which the base of the Brookian section attained that transformation ratio was estimated for each of the fifty synthetic wells in the study area, and Fig. HG19 is a contour map of that age.

These modeling results suggest that the onset of oil generation migrated to the north and west through Tertiary time. As illustrated by Fig. HG19, a 40 Ma (late Eocene) contour line trends from the southwest corner of the ANWR 1002 area northeastward to the eastern shore of Camden Bay, approximately parallel to the trend of the Marsh Creek anticline. A 30 Ma (mid Oligocene) contour follows a generally similar trend, except that it displays a prominent northwestward budge near the western border of the 1002 area. Contour lines representing the onset of the main phase of oil generation at 20 (early Miocene), 10 (late Miocene), and 0 Ma trend northward from the area of the Beli Unit 1 well and wrap around the east-plunging nose of the Mikkelsen high in the Point Thomson area. This analysis suggests that the base of the

Brookian section has not yet reached the onset of the main phase of oil generation west of the zero contour.

The end of the main phase of oil generation commonly is defined as a transformation ratio of 0.65. The age at which the base of the Brookian section attained that transformation ratio was estimated for each of the fifty synthetic wells in the study area, and Fig. HG20 is a contour map of that age.

Three contour lines (40, 30, and 20 Ma) trend from southwest to northeast across the entire study area, approximately parallel to the Marsh Creek anticline (Fig. HG20). Contours representing 10 Ma and 0 Ma, and a contour indicating where the onset of the main phase of oil generation has not yet been reached (contour labeled "N") display patterns that are more variable locally. Those contours appear to reflect the influence of the Mikkelsen high and subtle thickness variations within the Brookian section.

The contour patterns shown in Figs. HG19 and HG20 suggest that the timing of oil generation was influenced significantly by the sequence stratigraphic evolution of the area. In an area parallel to and extending approximately five to ten miles north of the Marsh Creek anticline, the base of the Brookian section passed through the main phase of oil generation during late Eocene through early Miocene time (~40 to ~20 Ma). This pattern suggests that the main phase of oil generation was influenced primarily by burial related to the south-southeastward thickening wedge of strata represented by Brookian sequences F (Paleocene - Fig. BSG6) and C (Eocene - Fig. BSG8) of Houseknecht and Schenk (Chap. BS). The accumulation of a significant thickness of Paleocene and Eocene strata buried the model horizon to depths and temperatures where oil generation either occurred during those times or occurred shortly thereafter as the overlying wedge of northward-thickening Oligocene strata was deposited.

In contrast, the area to the north (including the northwest corner of the ANWR 1002 area, adjacent State lands, and State waters) is characterized by contours that strike north-south, wrap around the Mikkelsen high, and display significant local variation in trend. In this part of the study area, the main phase of oil generation during Miocene through Holocene time appears to have been influenced primarily by burial related to the northward thickening wedge of strata represented by Brookian sequences B (Oligocene - Fig. BSG9) and A (Miocene - Fig. BSG10) of Houseknecht and Schenk (Chap. BS).

We believe that if data were incorporated from the Federal offshore area, the base of the Brookian section would be characterized by northward increasing ages of the main phase of oil generation (e.g., the 30 and 40 Ma contours in Fig. HG19 would wrap around to the west and parallel the 0, 10, and 20 Ma contours). This inference is based on published seismic data (e.g., Craig and others, 1985; Grantz and others, 1994) that illustrate thickening in an offshore direction of Brookian strata that appear to correlate with Eocene and perhaps older depositional sequences mapped by Houseknecht and Schenk (Chap. BS). In this context, a broader view of the timing of oil generation in the region suggests that the Mikkelsen high represents a focus of relatively recent oil generation and that the age of oil generation near the base of the Brookian section increases southward, eastward, and northward away from the Mikkelsen high.

It should be emphasized that this entire analysis is based on modeling oil generation at the base of the Brookian section, and that progressively younger Brookian strata would have reached onset and end of the main phase of oil generation at progressively younger ages.

The maps bracketing the age of the main phase of oil generation (Figs. HG19 and HG20) suggest favorable timing between oil generation, reservoir accumulation, and trap formation throughout the undeformed part of the ANWR 1002 area. Reservoirs beneath the Brookian section (including the Thomson sand, Kemik Sandstone, and Franklinian "sequence"; Bird, Chap. GG; Schenk and Houseknecht, Chap. TK) and within the Paleocene and Eocene portion of the Brookian section obviously pre-date oil generation throughout the undeformed part of the ANWR 1002 area. And, although Oligocene and Miocene reservoirs may post-date the main phase of oil generation in parts of the study area, it is likely that the timing of oil generation from source rocks above the base of the Brookian section (e.g., those associated with the Canning - Sagavanirktok petroleum system; Magoon and others, Chap. PS; Houseknecht and Schenk, Chap. BS) was favorable to charge those reservoirs (e.g., Figs. HG14 and HG16). Inasmuch as most traps in the undeformed part of the ANWR 1002 area are either exclusively stratigraphic or partly stratigraphic in nature, the same line of reasoning suggests favorable timing between trap formation and oil generation.

CONCLUSIONS

Seismic stratigraphy provides a robust framework for modeling the burial, thermal, and oil generation history of the undeformed part of the ANWR 1002 area. Temperature and vitrinite reflectance data from exploration wells located west of the ANWR 1002 area were used to constrain model values of heat flow. Model results for current heat flow based on analysis of bottom-hole temperatures are incongruent with vitrinite reflectance data if those heat flows are applied to the entire burial history of Brookian strata. Therefore, heat flow values were held constant through time and their magnitude was adjusted to achieve a match between vitrinite reflectance calculated using a kinetic model and vitrinite reflectance measured from well samples. This approach results in the use of heat flow values lower than commonly reported for similar geologic settings.

Modeling results suggest that the base of the Brookian section in the undeformed part of the ANWR 1002 area is characterized by vitrinite reflectance values that fall within the upper part of the oil generation window or within the gas generation window. This suggests that oil generation near the base of the Brookian section is essentially complete and that most of the overlying strata are characterized by thermal maturities favorable for the preservation of any oil that migrated from deeper in the section.

Modeled transformation ratios similarly suggest that oil generation is mostly or entirely complete near the base of the Brookian section throughout the study area. Modeling the age of the main phase of oil generation suggests that the Mikkelsen high represents a focus of relatively recent oil generation and that the age of oil generation increases southward, eastward, and northward away from the Mikkelsen high. Timing of the main phase of oil generation at the base of the Brookian section ranges from ~40 Ma along the trend of the Marsh Creek anticline to 0 Ma near the crest of the Mikkelsen high.

Modeling results suggest that the undeformed part of the ANWR 1002 area is characterized by favorable timing among oil generation, reservoir deposition, and trap formation. Most importantly, the age of the main phase of oil generation decreases systematically northward from ~40 Ma at the Marsh Creek anticline to 0 Ma at the Mikkelsen high. In addition, source rocks thought to be present higher in the Brookian section (i.e., source rocks associated with the Canning - Sagavanirktok petroleum system) would have

entered the main phase of oil generation at progressively younger ages. Thus, even the youngest potential reservoirs and traps identified in this assessment (Miocene aged sandstones in sequence A of Houseknecht and Schenk, Chap. BS) have favorable charge potential based on this analysis.

Use of higher heat flow values in modeling would increase the calculated values of vitrinite reflectance, transformation ratio, and ages of onset and end of the main phase of oil generation. Such increases would shift some Brookian strata out of the oil window and into the gas window, and would yield ages for the main phase of oil generation that pre-date the deposition of some reservoir units and pre-date development of some traps.

ACKNOWLEDGMENTS

We appreciate the contributions of Ken Bird and Phil Nelson. Incisive reviews by Charles Barker, Vito Nuccio, and Les Magoon helped clarify our presentation.

REFERENCES

Anders, D.E., Magoon, L.B., and Lubeck, C., 1987, Geochemistry of surface oil shows and potential source rocks: *in* Bird, K.J., and Magoon, L.B. (eds.), 1987, Petroleum Geology of the Northern Part of the Arctic National Wildlife Refuge, Northeastern Alaska, U.S. Geological Survey, Bulletin 1778, p. 181-198.

Bird, K.J., and Molenaar, C.M., 1987, Chapter 5. Stratigraphy: *in* Bird, K.J., and Magoon, L.B. (eds.), 1987, Petroleum Geology of the Northern Part of the Arctic National Wildlife Refuge, Northeastern Alaska, U.S. Geological Survey, Bulletin 1778, p. 37-59.

Blackwell, D.D., and Steele, J.L., 1989, Thermal conductivity of sedimentary rocks: Measurement and significance: in Naeser, N.D., and McCulloh, T.H. (eds.), Thermal History of Sedimentary Basins, Methods and Case Histories, Springer - Verlag, New York, p. 13-36.

Brewer, M.C., 1987, Surficial geology, permafrost, and physical processes: *in* Bird, K.J., and Magoon, L.B. (eds.), 1987, Petroleum Geology of the

Click here or on this symbol in the toolbar to return.

Northern Part of the Arctic National Wildlife Refuge, Northeastern Alaska, U.S. Geological Survey, Bulletin 1778, p. 27-36.

Burnham, A.K., and Sweeney, J.J., 1989, A chemical kinetic model of vitrinite maturation and reflectance: Geochimica et Cosmochimica Acta, v. 53, p. 2649-2657.

Craig, J.D., Sherwood, K.W., and Johnson, P.P., 1985, Geologic report for the Beaufort Sea planning area, Alaska: Regional geology, petroleum geology, environmental geology: Minerals Management Service, OCS Report, MMS 85-0111, 192 p.

Deming, D., Sass, J.H., Lachenbruch, A.H., and De Rito, R.F., 1992, Heat flow and subsurface temperature as evidence for basin-scale ground-water flow, North Slope of Alaska: Geological Society of America Bulletin, v. 104, p. 528-542.

Grantz, A., May, S.D., and Hart, P.E., 1994, Geology of the Arctic continental margin of Alaska: *in* Plafker, G., and Berg, H.C. (eds.), The Geology of Alaska, The Geology of North America, Geological Society of America, v. G-1, p. 17-48.

Gretener, P.E., 1981, Geothermics: Using temperature in hydrocarbon exploration: American Association of Petroleum Geologists, Education Course Note Series 17, 170 p.

Habicht, J.K.A., 1979, Paleoclimate, Paleomagnetism, and Continental Drift: American Association of Petroleum Geologists Studies in Geology No. 9, 31 p.

Lachenbruch, A.H., and Marshall, B.V., 1986, Changing climate: Geothermal evidence from permafrost in the Alaskan arctic: Science, v. 234, p. 689-696.

Law, B.E., Nuccio, V.F., and Barker, C.E., 1989, Kinky vitrinite reflectance well profiles: Evidence of paleopore pressure in low-permeability, gas-bearing sequences in Rocky Mountain foreland basins: American Association of Petroleum Geologists Bulletin, v. 73, p. 999-1010.

Magoon, L.B., Woodward, P.V., Banet, A.C., Jr., Griscom, S.B., and Daws, T.A., 1987, Chapter 11. Thermal maturity, richness, and type of organic matter of source-rock units: *in* Bird, K.J., and Magoon, L.B. (eds.), 1987, Petroleum Geology of the Northern Part of the Arctic National Wildlife Refuge, Northeastern Alaska, U.S. Geological Survey, Bulletin 1778, p. 127-179.

O'Sullivan, P.B., Green, P.F., Bergman, S.C., Decker, J., Duddy, I.R., Gleadow, A.J.W., and Turner, D.L., 1993, Multiple phases of Tertiary uplift and erosion in the Arctic National Wildlife Refuge, Alaska, revealed by apatite fission track analysis: American Association of Petroleum Geologists Bulletin, v. 77, p. 359-385.

Parrish, J.T., and Barron, E.J., 1986, Paleoclimates and Economic Geology: SEPM Short Course Notes No. 18, 162 p.

Sweeney, J.J., and Burnham, A.K., 1990, Evaluation of a simple model of vitrinite reflectance based on chemical kinetics: Association of Petroleum Geologists Bulletin, v. 74, p. 1559-1570.

Waples, D.W., 1994, Maturity modeling: Thermal indicators, hydrocarbon generation, and oil cracking: in Magoon, L.B., and Dow, W.G. (eds.), The Petroleum System -- From Source to Trap, American Association of Petroleum Geologists Memoir 60, p. 285-306.

Click here or on this symbol in the toolbar to return.

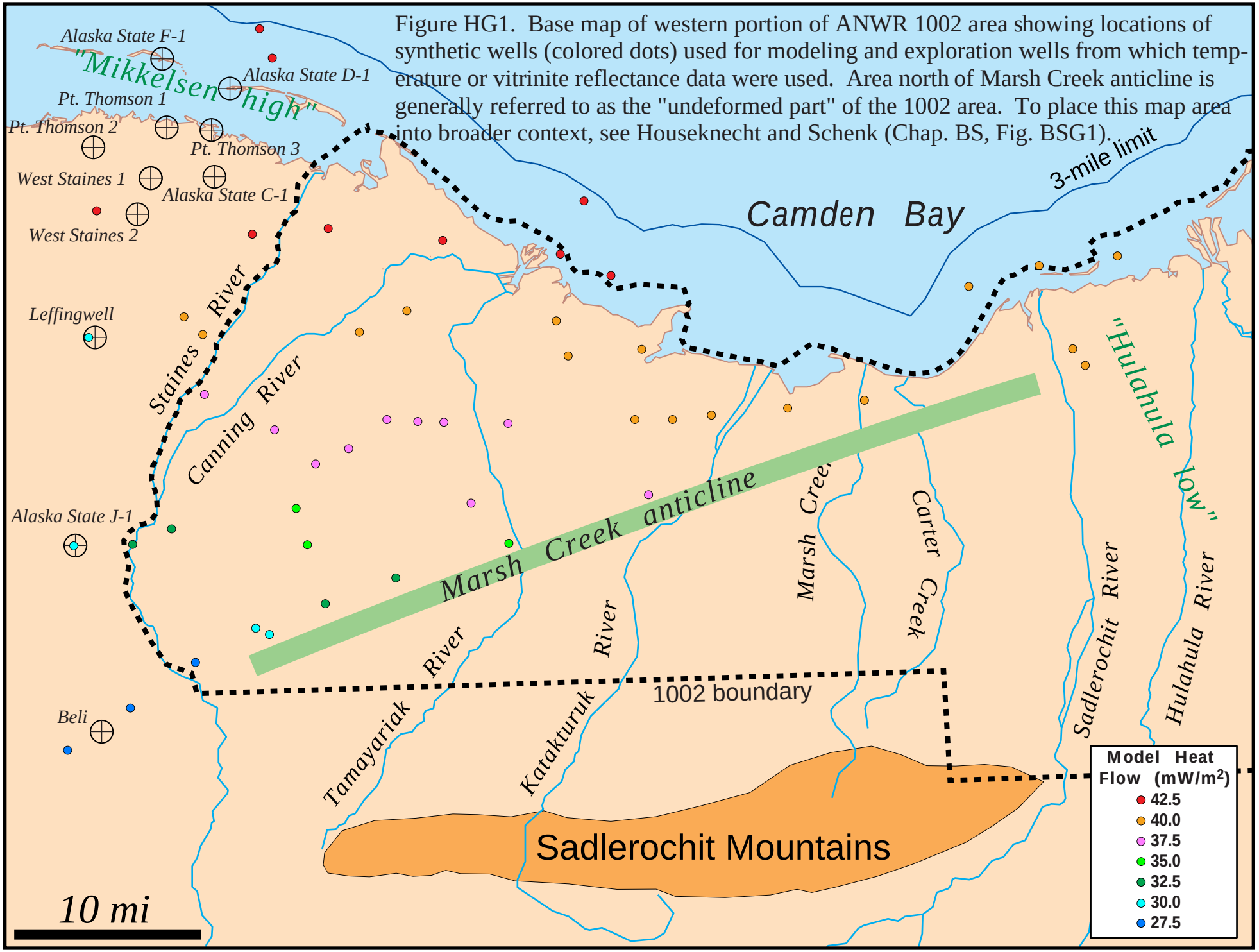

Figure HG1. Base map of western portion of ANWR 1002 area showing locations of synthetic wells (colored dots) used for modeling and exploration wells from which temperature or vitrinite reflectance data were used. Area north of Marsh Creek anticline is generally referred to as the "undeformed part" of the 1002 area. To place this map area into broader context, see Houseknecht and Schenk (Chap. BS, Fig. BSG1).

Click here or on this symbol
in the toolbar to return.

Figure HG2. Depth vs. vitrinite reflectance plot for Point Thomson Unit 1 well (see Fig. HG1 for location). Blue line is eyeball approximation of gradient inferred to represent thermal maturation resulting from burial at this location and red line is inferred to represent recycled vitrinite. Approximate position of Lower Cretaceous Unconformity (LCU) shown to approximate "base of Brookian section" as modeled. Black symbols at sides indicate casing points.

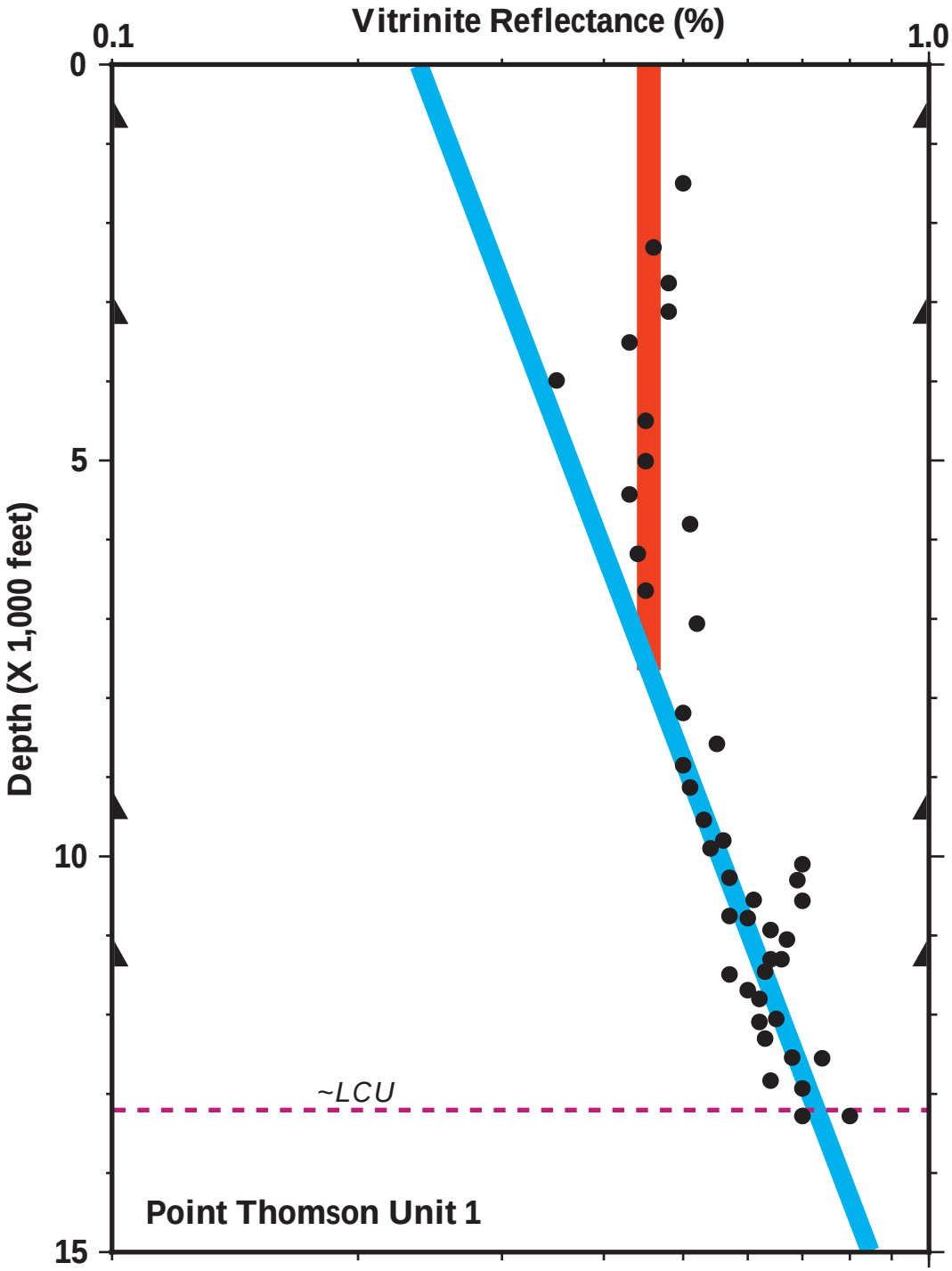

Figure HG3. Depth vs. vitrinite reflectance plot for Point Thomson Unit 3 well (see Fig. HG1 for location). Blue line is eyeball approximation of gradient inferred to represent thermal maturation resulting from burial at this location and red line is inferred to represent recycled vitrinite. Approximate position of Lower Cretaceous Unconformity (LCU) shown to approximate "base of Brookian section" as modeled. Black symbols at sides indicate casing points.

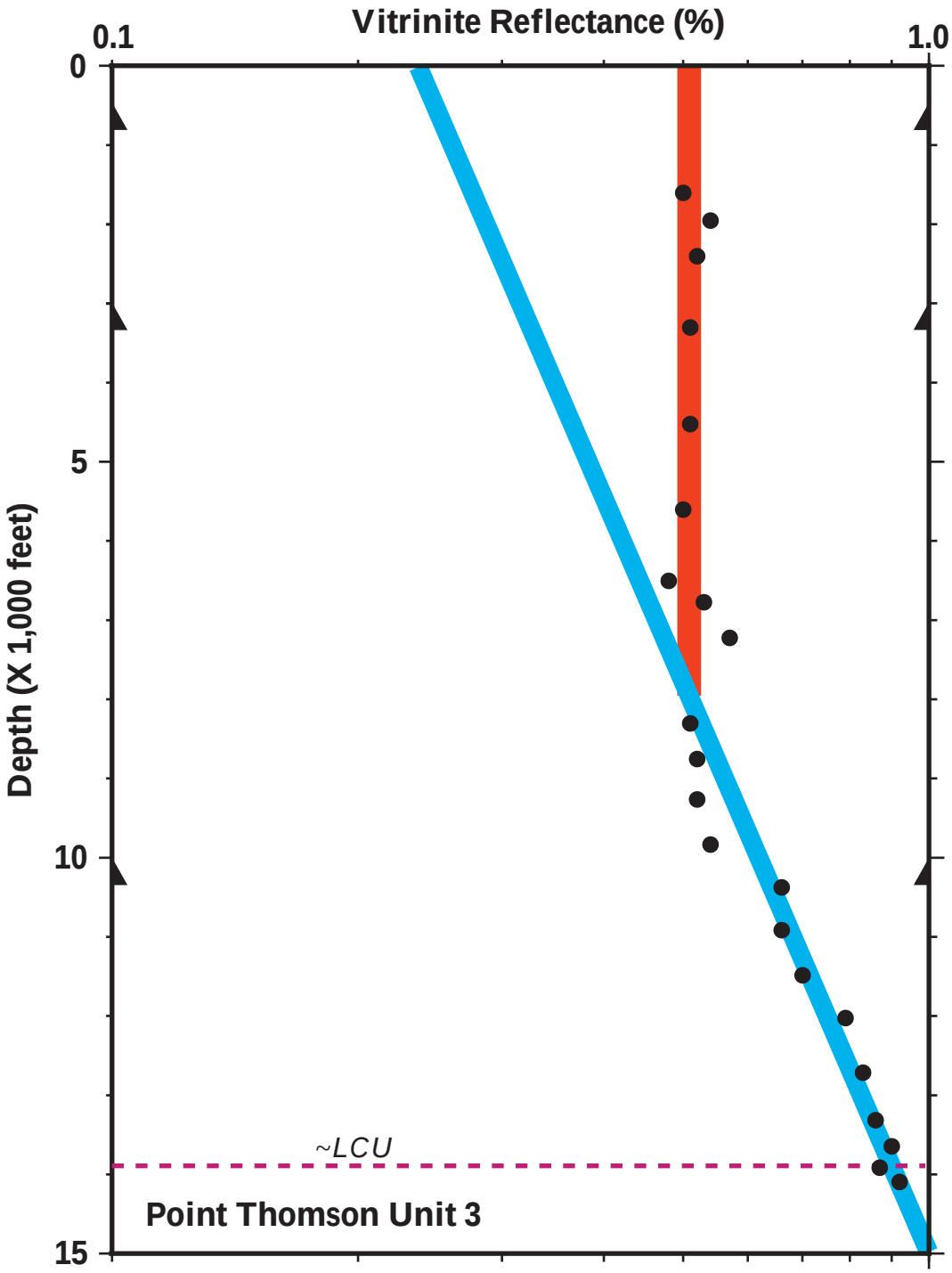

Figure HG4. Depth vs. vitrinite reflectance plot for Alaska State D-1 well (see Fig. HG1 for location). Blue line is eyeball approximation of gradient inferred to represent thermal maturation resulting from burial at this location and red line is inferred to represent recycled vitrinite. Approximate position of Lower Cretaceous Unconformity (LCU) shown to approximate "base of Brookian section" as modeled. Black symbols at sides indicate casing points.

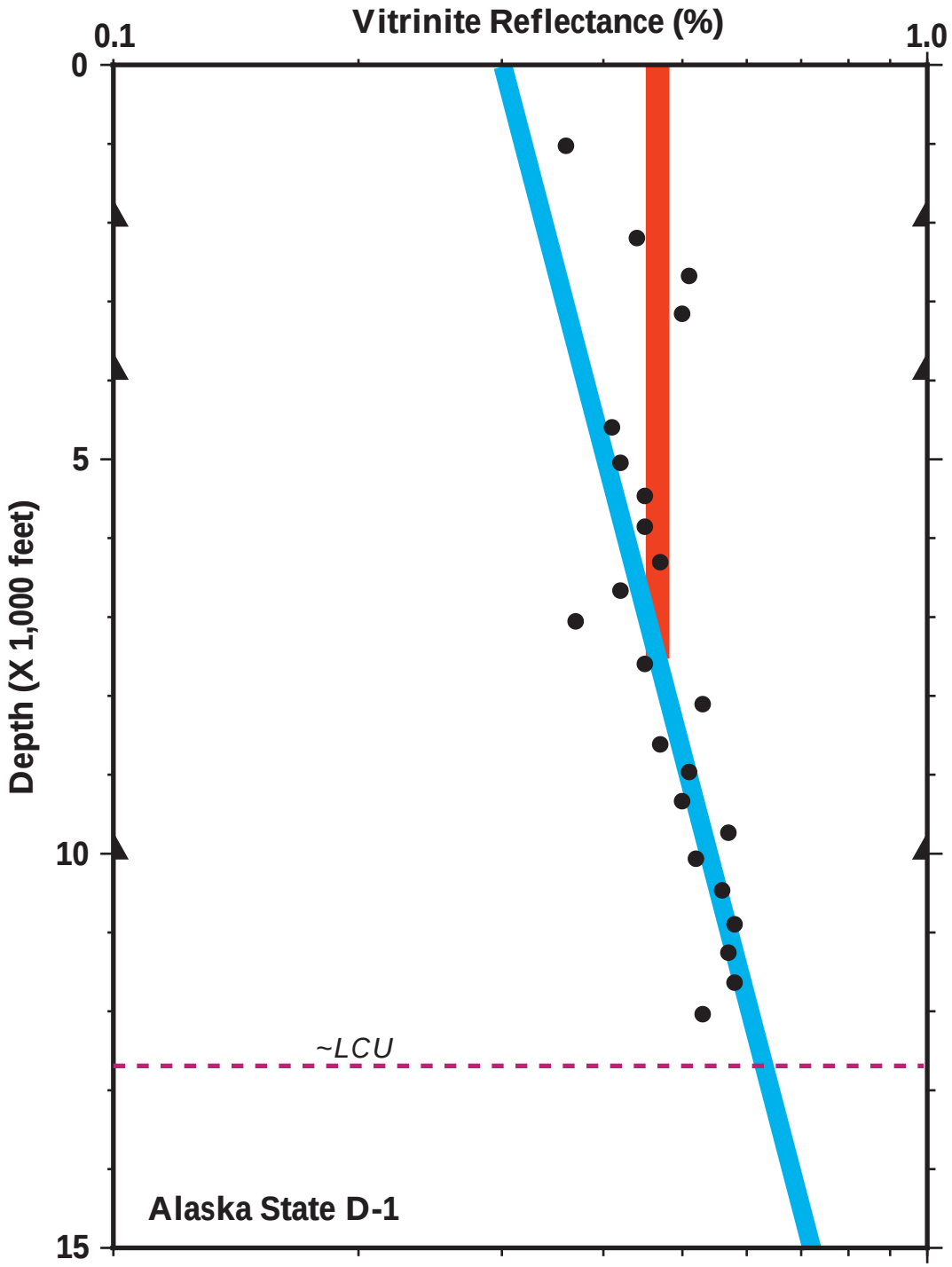

Figure HG5. Depth vs. vitrinite reflectance plot for Alaska State F-1 well (see Fig. HG1 for location). Blue line is eyeball approximation of gradient inferred to represent thermal maturation resulting from burial at this location and red line is inferred to represent recycled vitrinite. Approximate position of Lower Cretaceous Unconformity (LCU) shown to approximate "base of Brookian section" as modeled. Black symbols at sides indicate casing points.

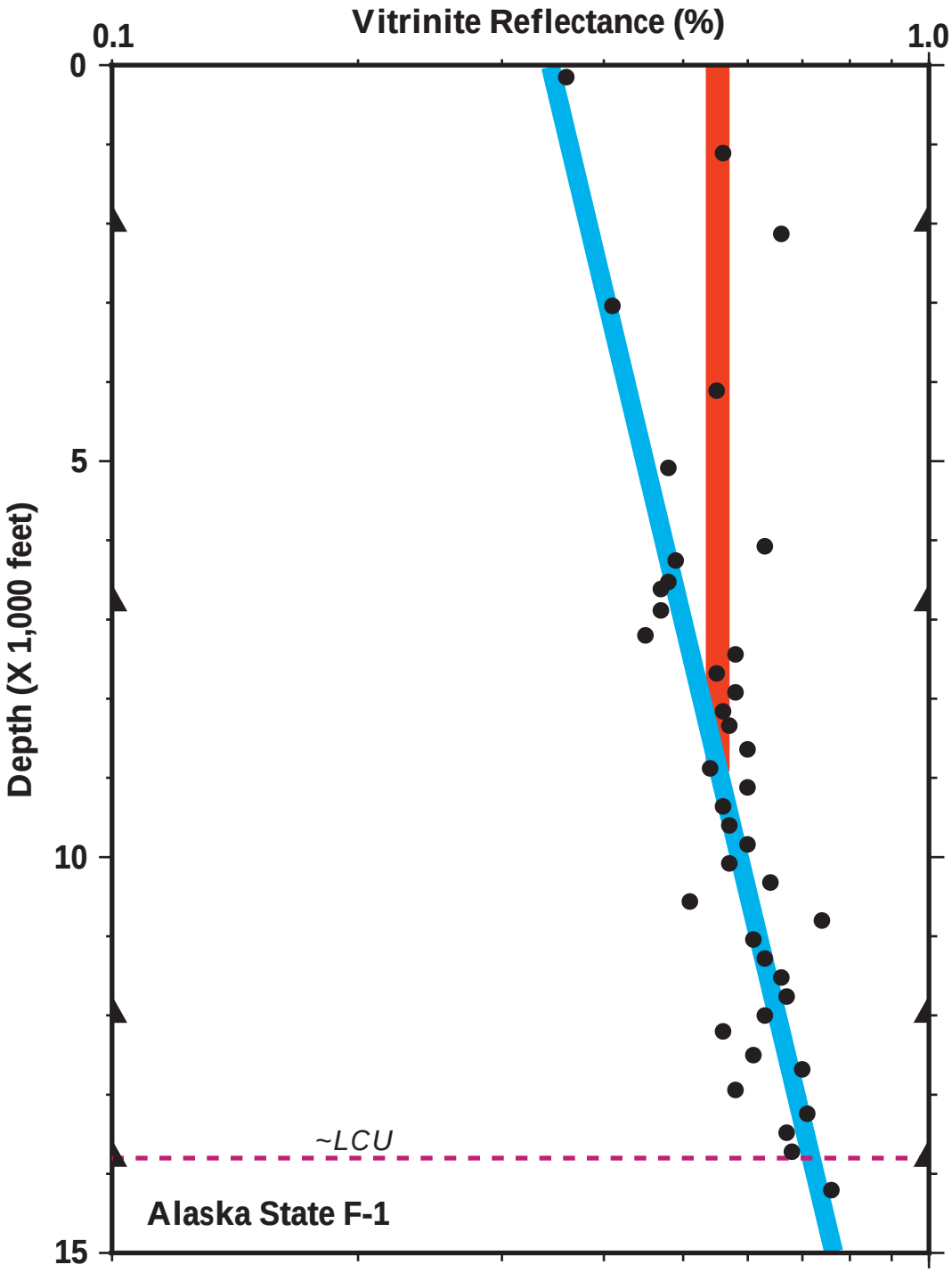

Figure HG6. Depth vs. vitrinite reflectance plot for West Staines State 2 well (see Fig. HG1 for location). Blue line is eyeball approximation of gradient inferred to represent thermal maturation resulting from burial at this location and red line is inferred to represent recycled vitrinite. Approximate position of Lower Cretaceous Unconformity (LCU) shown to approximate "base of Brookian section" as modeled. Data from this well are difficult to interpret because of extreme variation in reflectance values over short intervals of depth. Black symbols at sides indicate casing points.

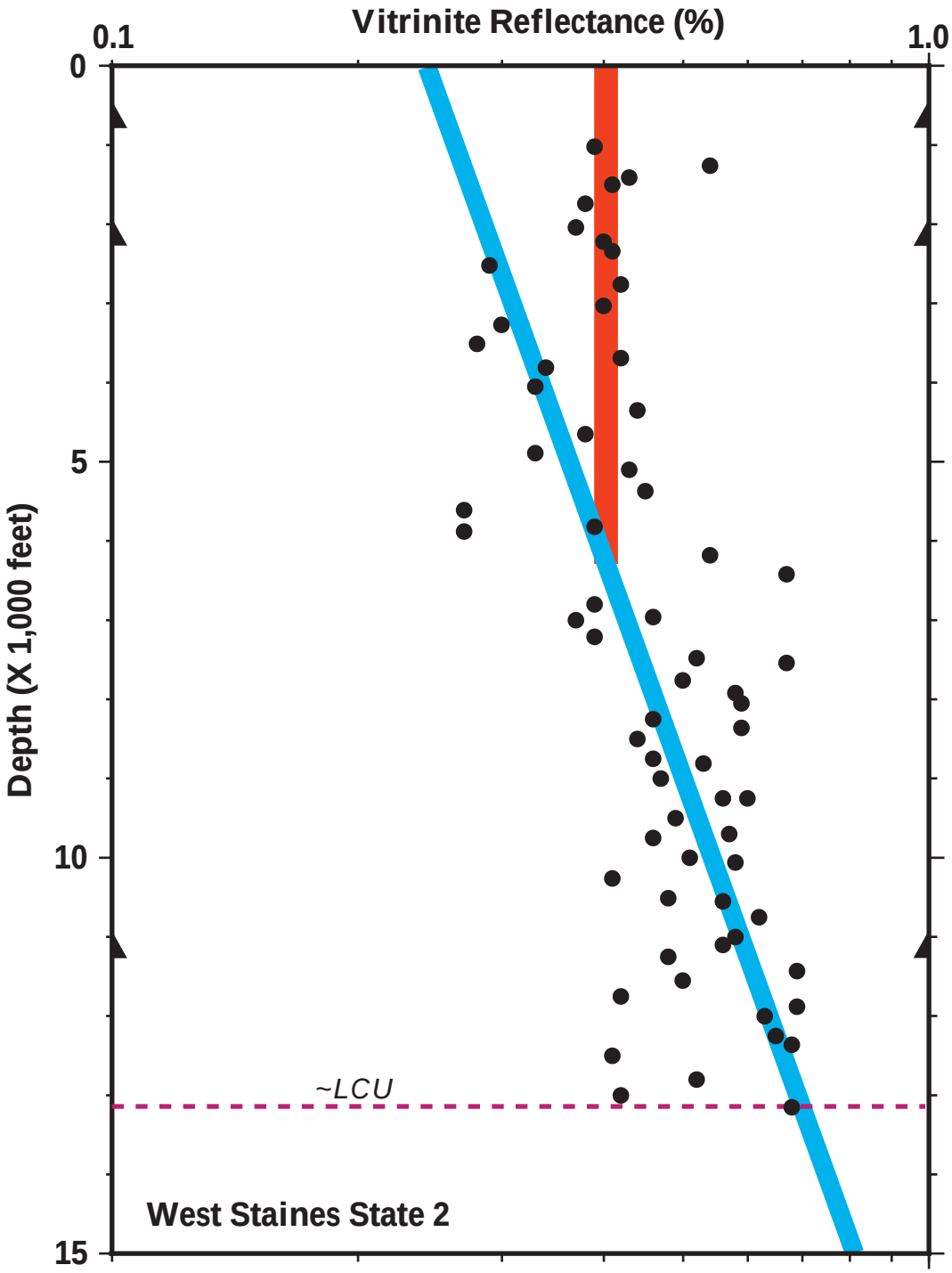

Click here or on this symbol
in the toolbar to return.

Figure HG7. Depth vs. vitrinite reflectance plot for E De K Leffingwell well (see Fig. HG1 for location). Blue line is eyeball approximation of gradient inferred to represent thermal maturation resulting from burial at this location and red dashed line is inferred to represent recycled vitrinite. Approximate position of Lower Cretaceous Unconformity (LCU) shown to approximate "base of Brookian section" as modeled. Black symbols at sides indicate casing points.

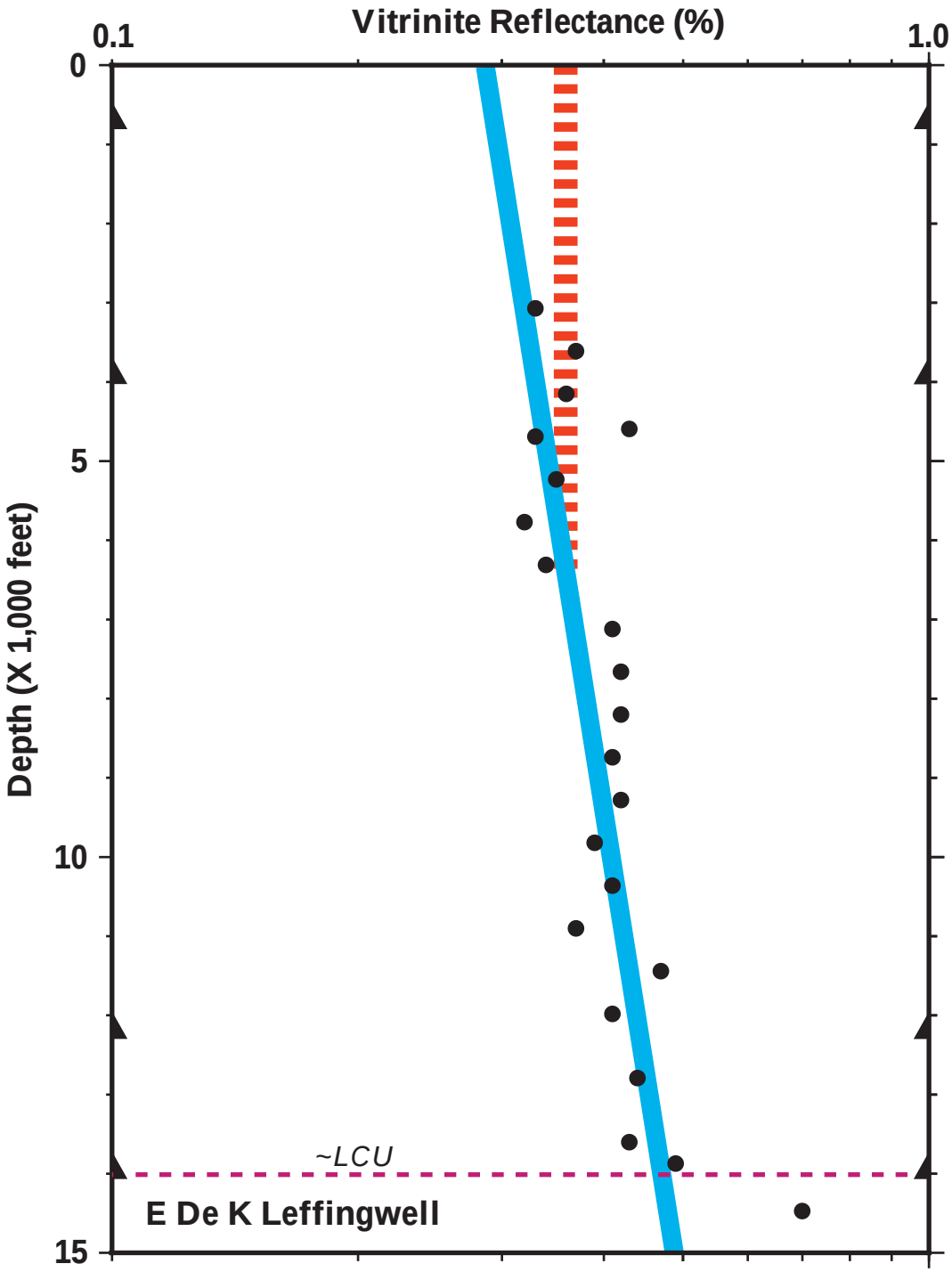

Figure HG8. Depth vs. vitrinite reflectance plot for Alaska State J-1 well (see Fig. HG1 for location). Blue line is eyeball approximation of gradient inferred to represent thermal maturation resulting from burial at this location and red dashed line is inferred to represent recycled vitrinite. Approximate position of Lower Cretaceous Unconformity (LCU) shown to approximate "base of Brookian section" as modeled. Black symbols at sides indicate casing points.

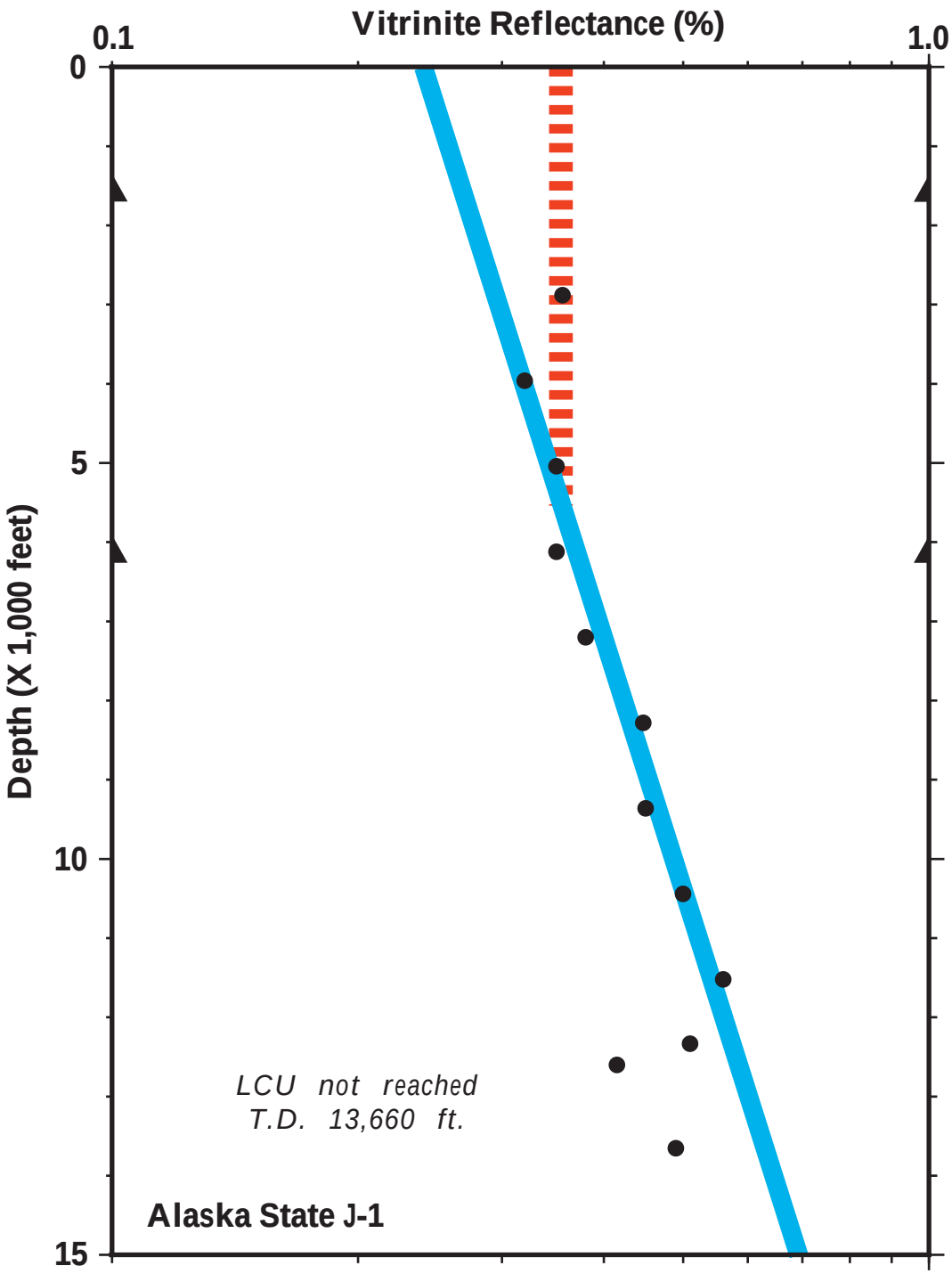

Figure HG9. Depth vs. vitrinite reflectance plot for Beli Unit 1 well (see Fig. HG1 for location). Blue line is eyeball approximation of gradient inferred to represent thermal maturation resulting from burial at this location and red dashed line is inferred to represent recycled vitrinite. Approximate position of Lower Cretaceous Unconformity (LCU) shown to approximate "base of Brookian section" as modeled. Black symbols at sides indicate casing points.

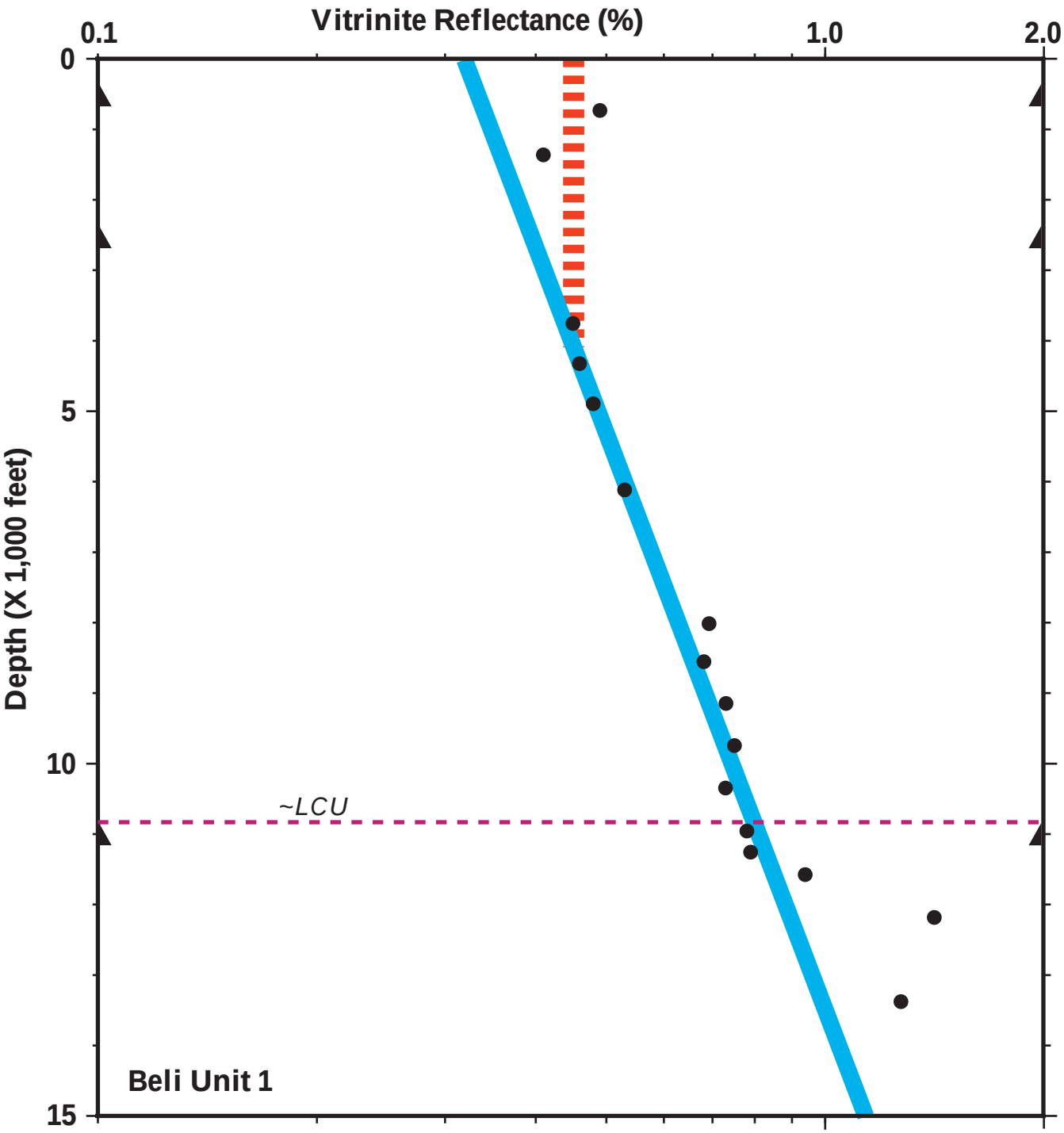

Figure HG10. Geohistory plot for synthetic well located in the Point Thomson area. Stratigraphic column is composed of sequences defined by Houseknecht and Schenk (Chap. BS). Known source rocks (e.g., Hue Shale) occur within sequence G, which was combined with the overlying sequence F for mapping purposes.

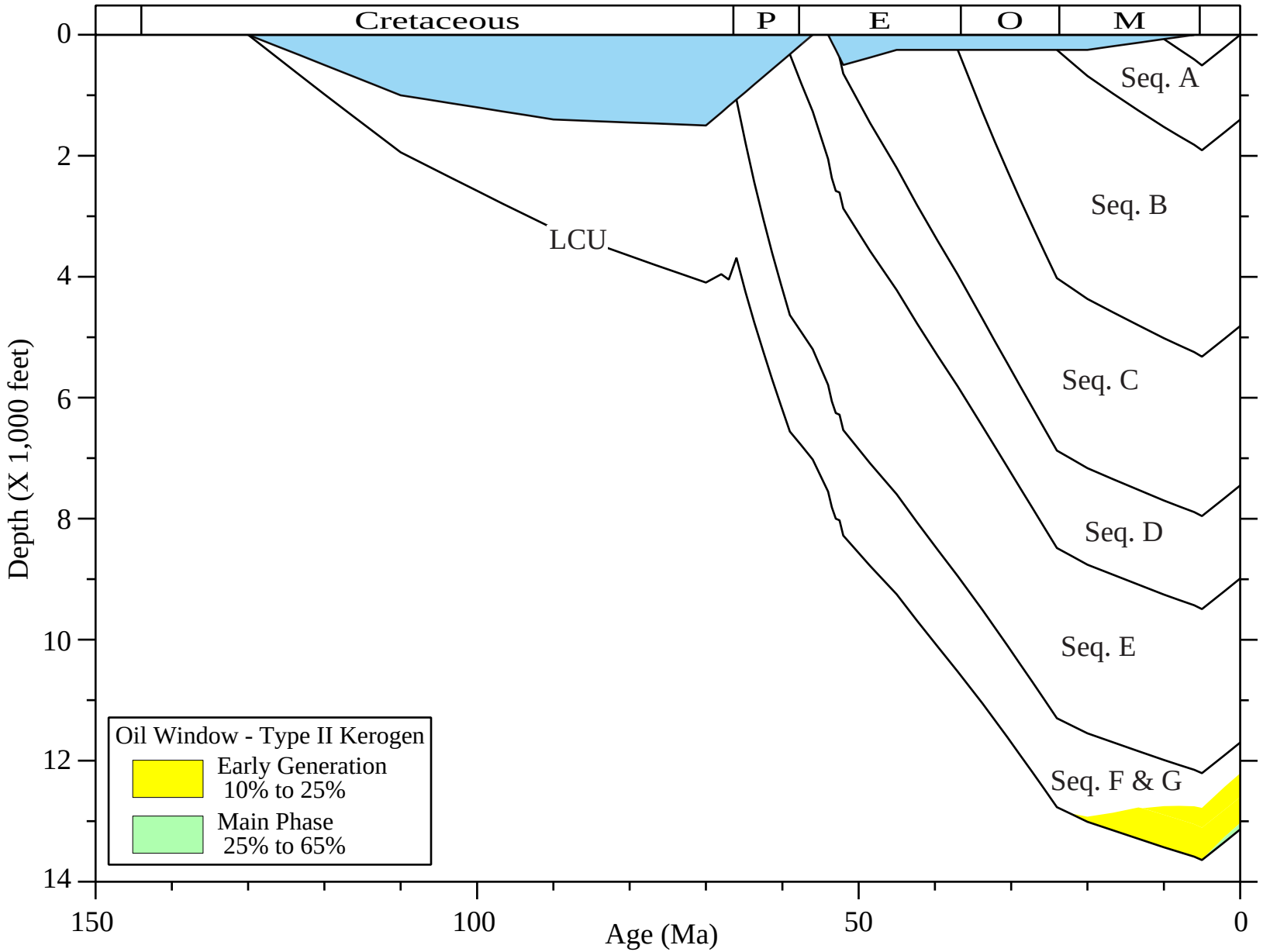

Click here or on this symbol
in the toolbar to return.

Figure HG11. Plot of depth vs. vitrinite reflectance for burial history model shown in Figure HG10 and using a heat flow of 42.5 mW/m^2. Blue line is model result calculated using vitrinite reflectance kinetics; blue X's are measured data from Point Thomson Unit 1 well. Note that colored areas define maturity windows, defined on basis of vitrinite reflectance, and do not correlate exactly with kinetic windows shown in Figures HG10 and HG12.

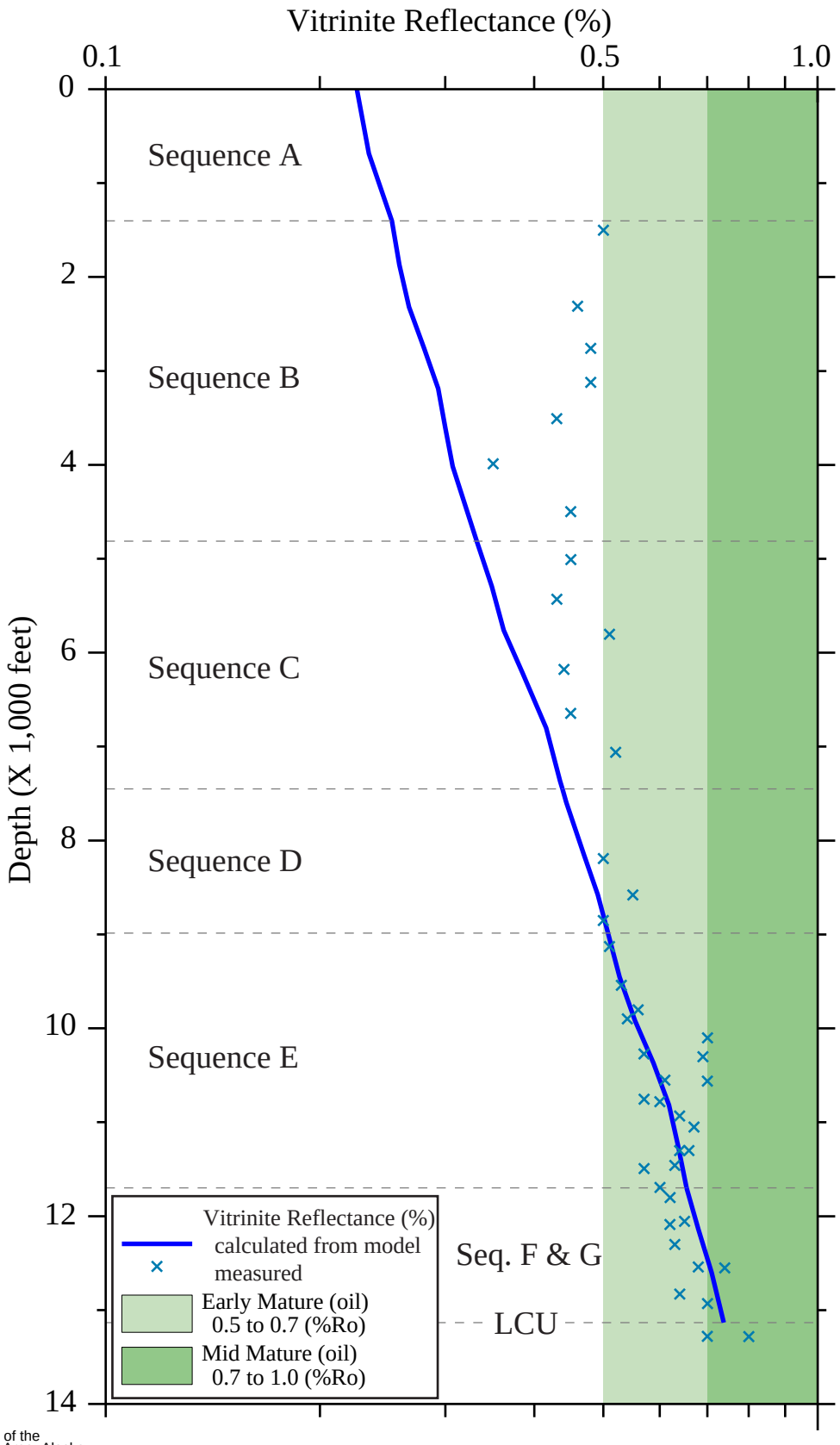

Figure HG12. Plot of age vs. transformation ratio for for geohistory model shown in Figure HG10 and using a heat flow of 42.5 mW/m^2. The red and blue curves represent the bottom and top stratigraphic boundaries, respectively, of combined sequence F & G (Houseknecht and Schenk, Chap. BS). Note that yellow and green windows are same kinetic windows shown in Figure HG10, which do not correlate exactly with maturity windows shown in Figures HG11.

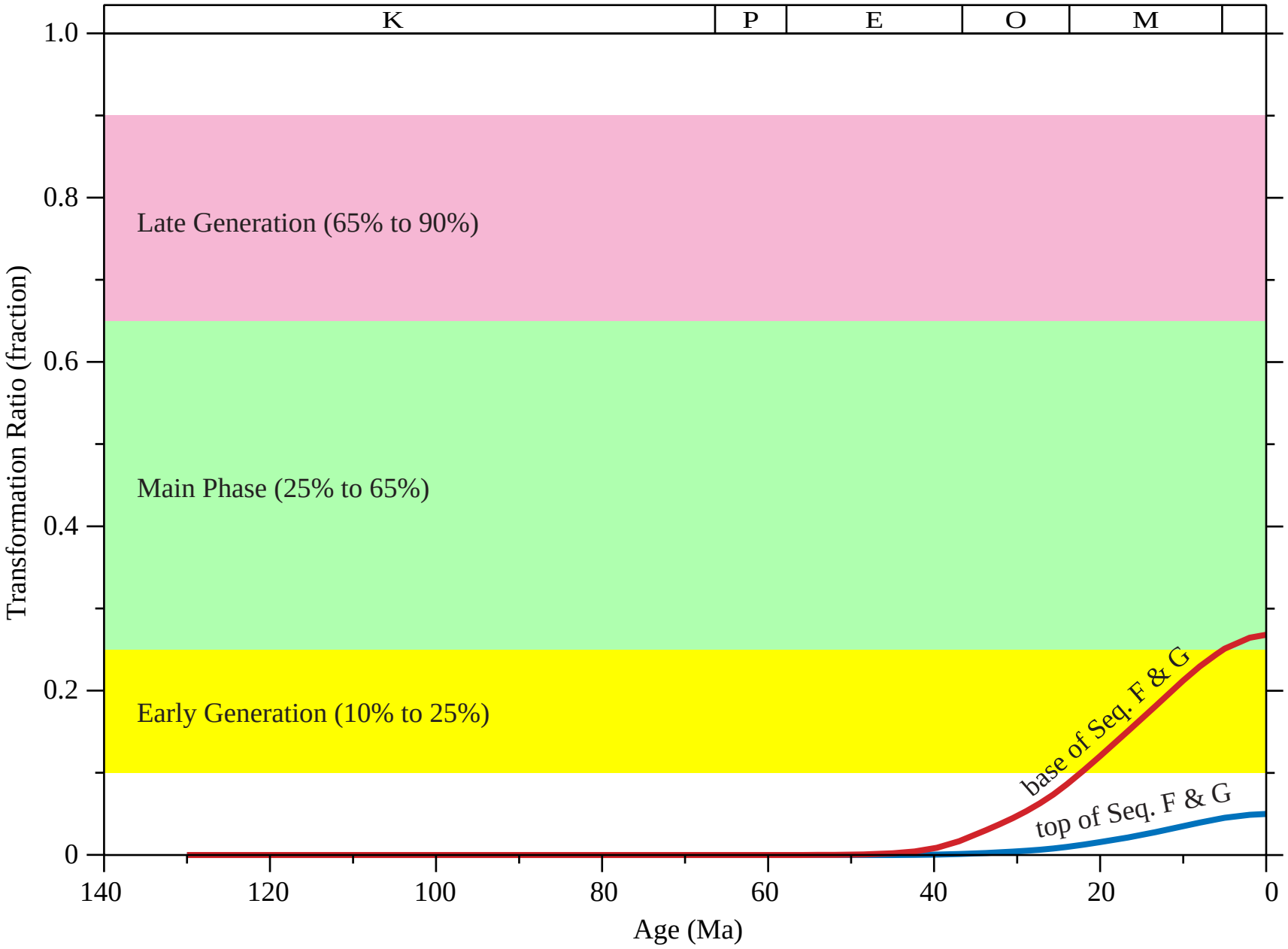

Figure HG13. Generalized isopach map showing approximate total thickness of Brookian strata.

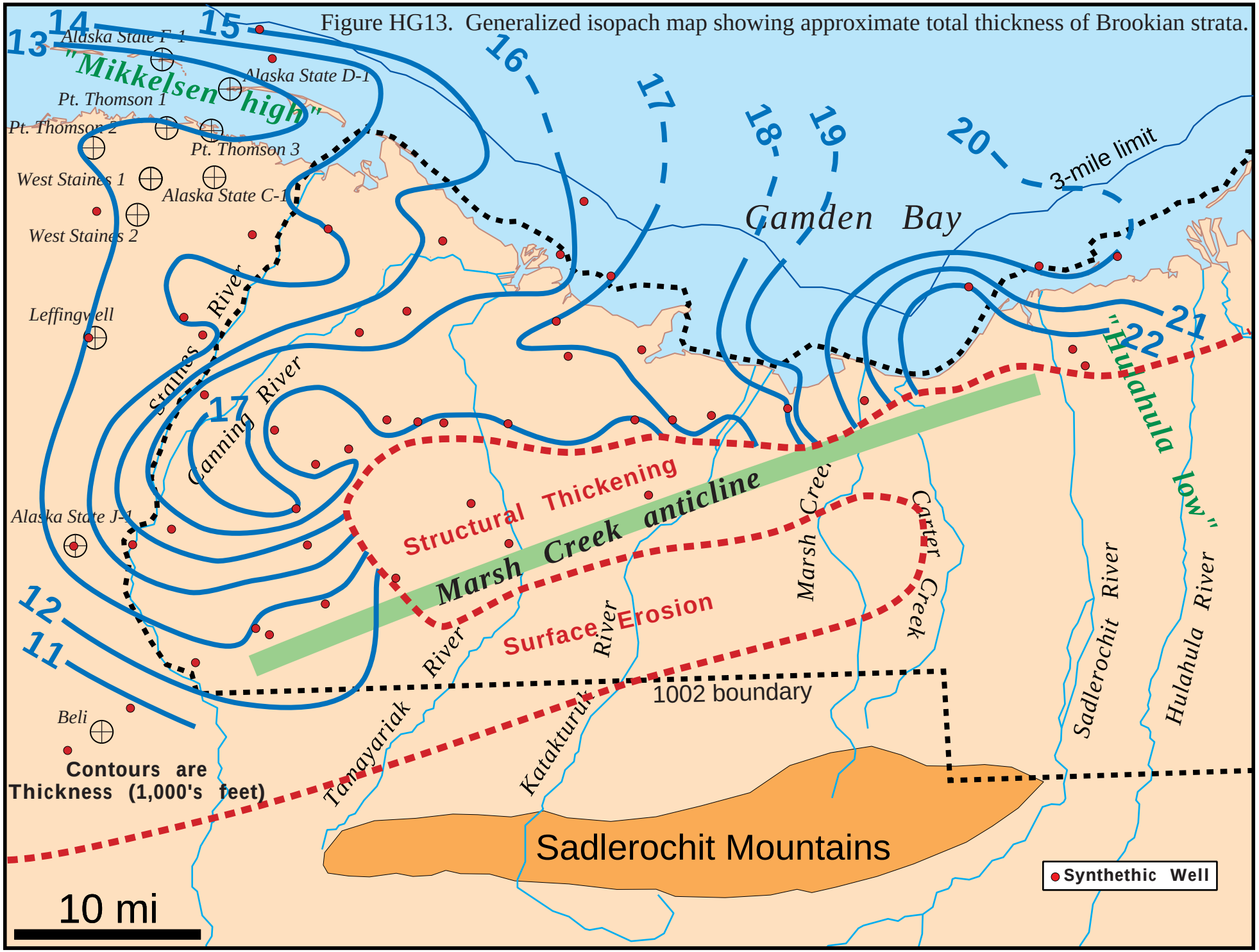

Figure HG14. Geohistory plot for synthetic well located along the western margin of the "Hulahula low", just south of Camden Bay (Fig. HG1). Stratigraphic column is composed of sequences defined by Houseknecht and Schenk (Chap. BS). Model assumes the presence of type II kerogen in sequence E and type III kerogen in sequence C. LCU = Lower Cretaceous Unconformity; BTU = basal Tertiary unconformity. Note depth scale is different than that of Fig. HG10.

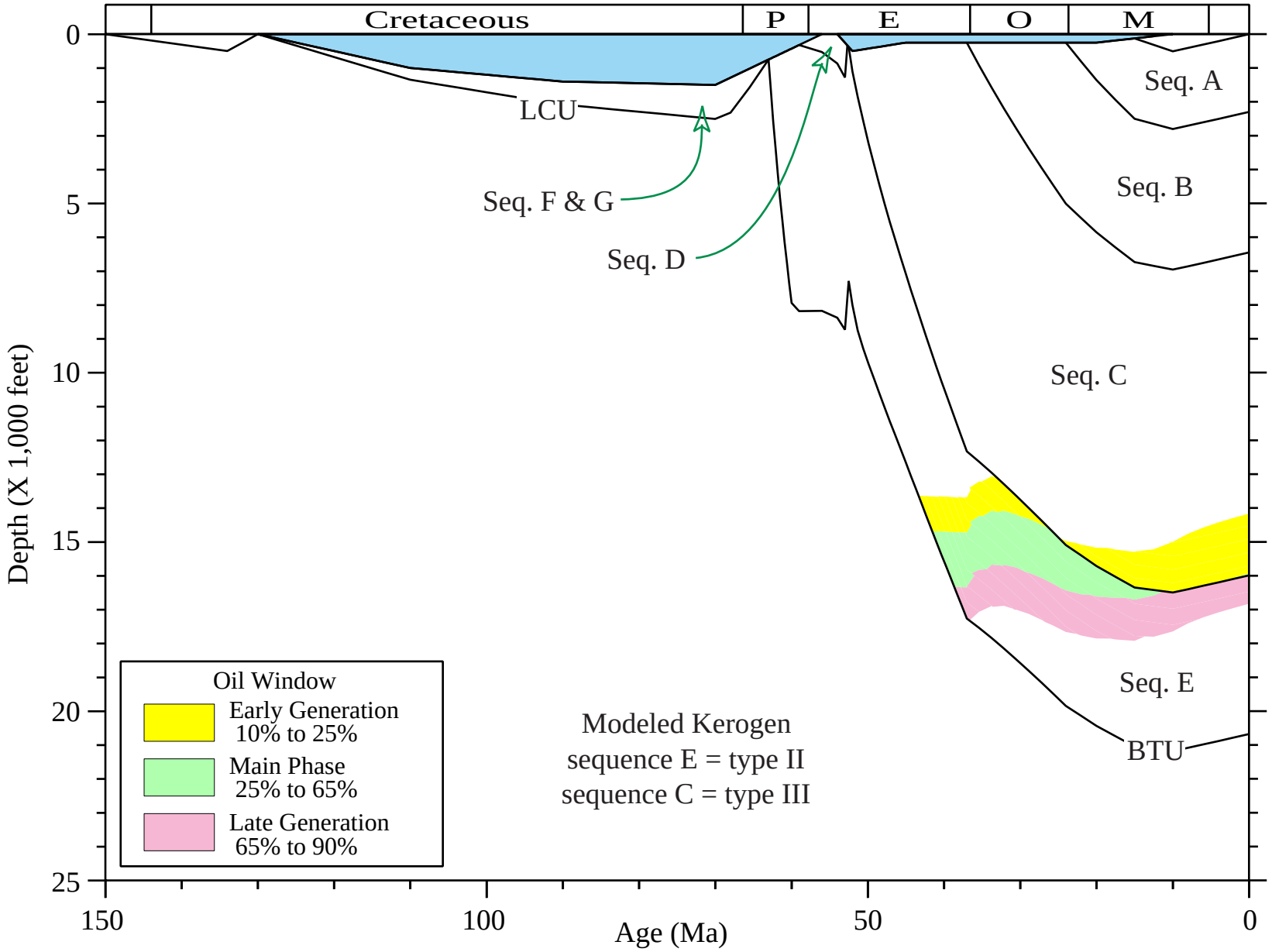

Figure HG15. Plot of depth vs. calculated vitrinite reflectance for burial history model shown in Figure HG14 and using a heat flow of 40 mW/m^2. Note that colored areas define maturity windows, defined on basis of vitrinite reflectance, and do not correlate exactly with kinetic windows shown in Figures HG14 and HG16.

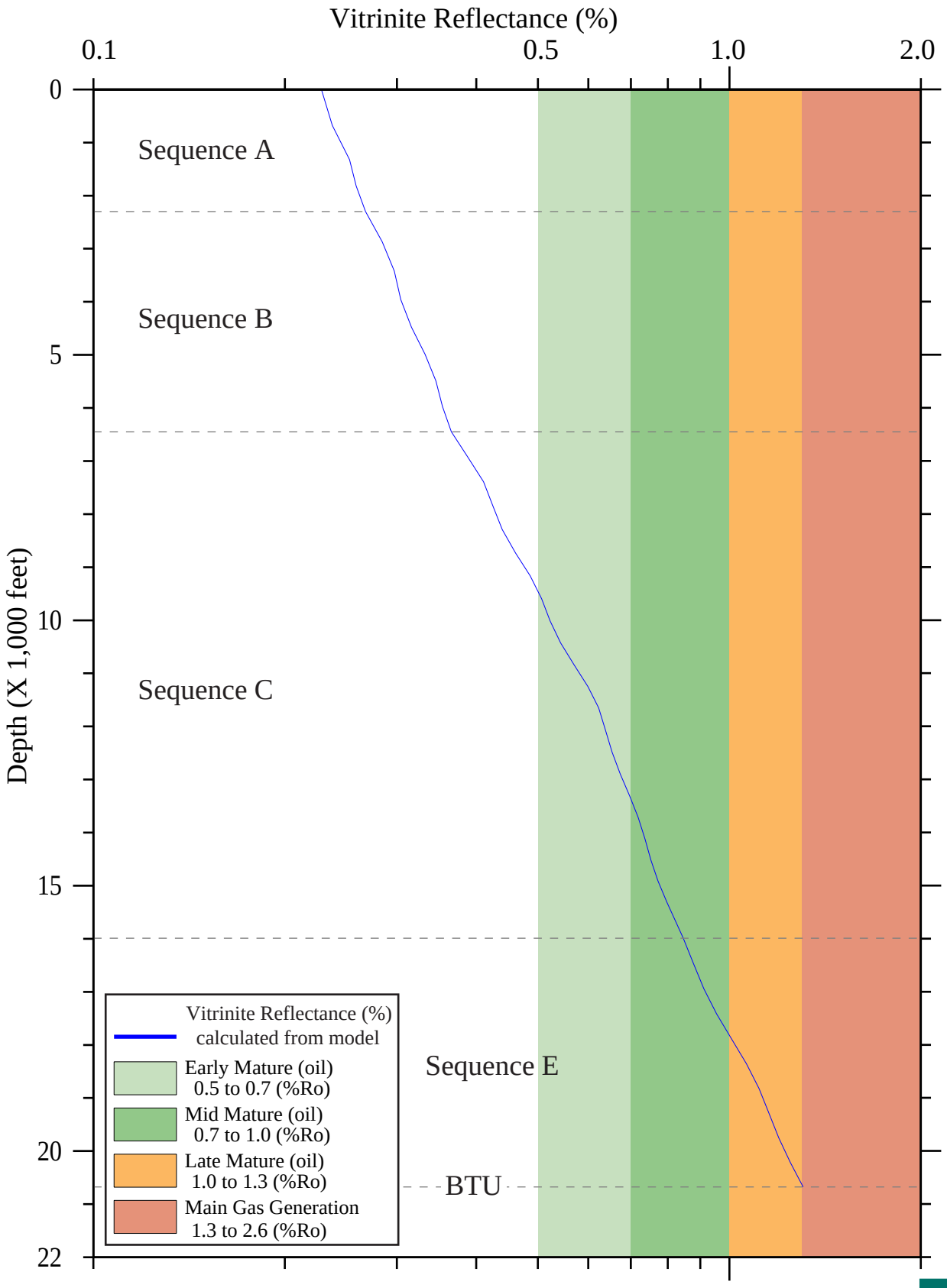

Figure HG16. Plot of age vs. transformation ratio for geohistory model shown in Figure HG14 and using a heat flow of 40 mW/m^2. The red and blue curves represent the base and top, respectively, of sequence E; the black curve represents the base of sequence C (Houseknecht and Schenk, Chap. BS). Model assumes the presence of type II kerogen in sequence E and type III kerogen in sequence C. Note that yellow and green windows are same kinetic windows shown in Figure HG14, which do not correlate exactly with maturity windows shown in Figures HG15.

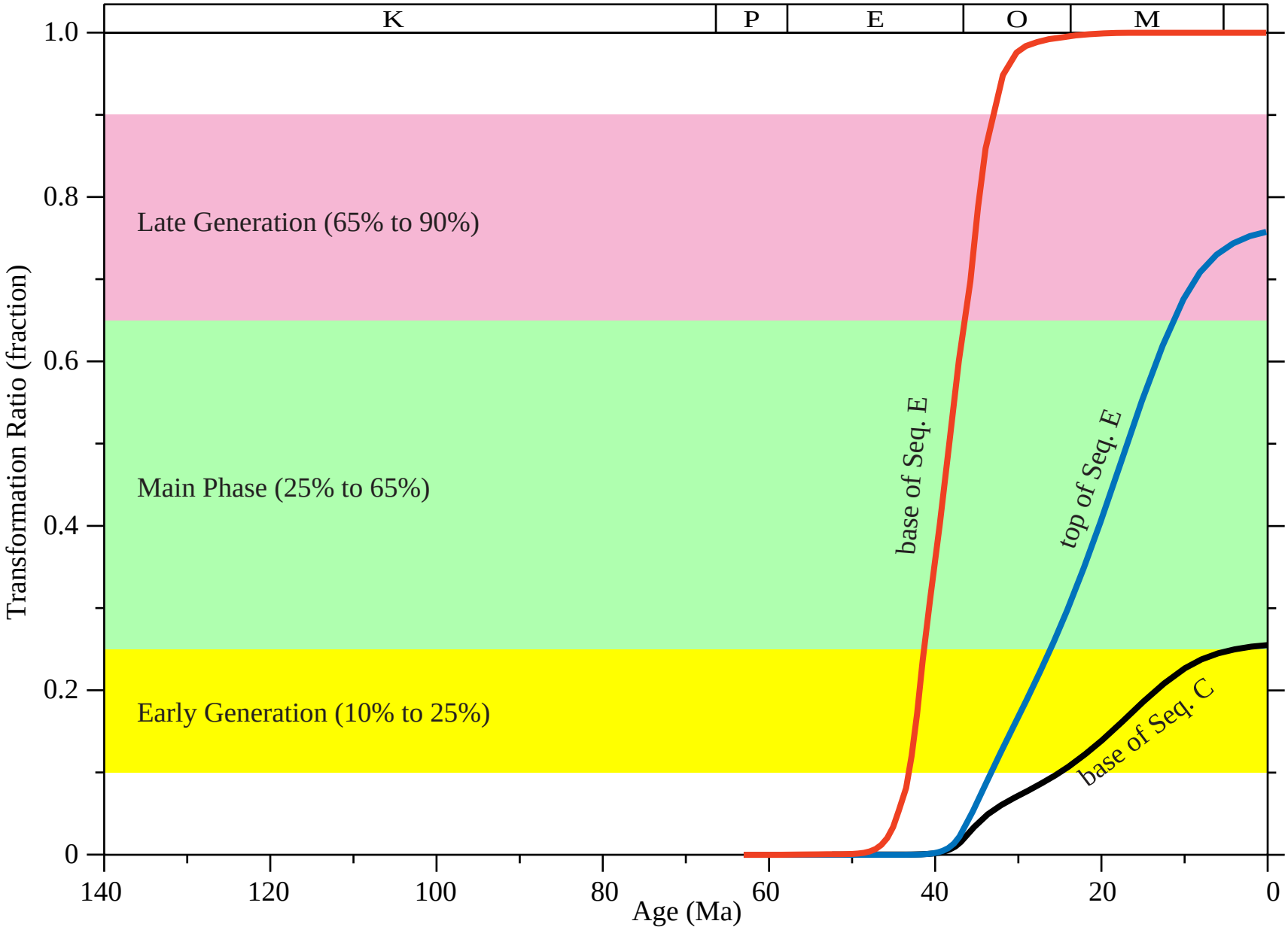

Figure HG17. Map of estimated vitrinite reflectance at base of Brookian section, calculated by burial and thermal history modeling as described in text.

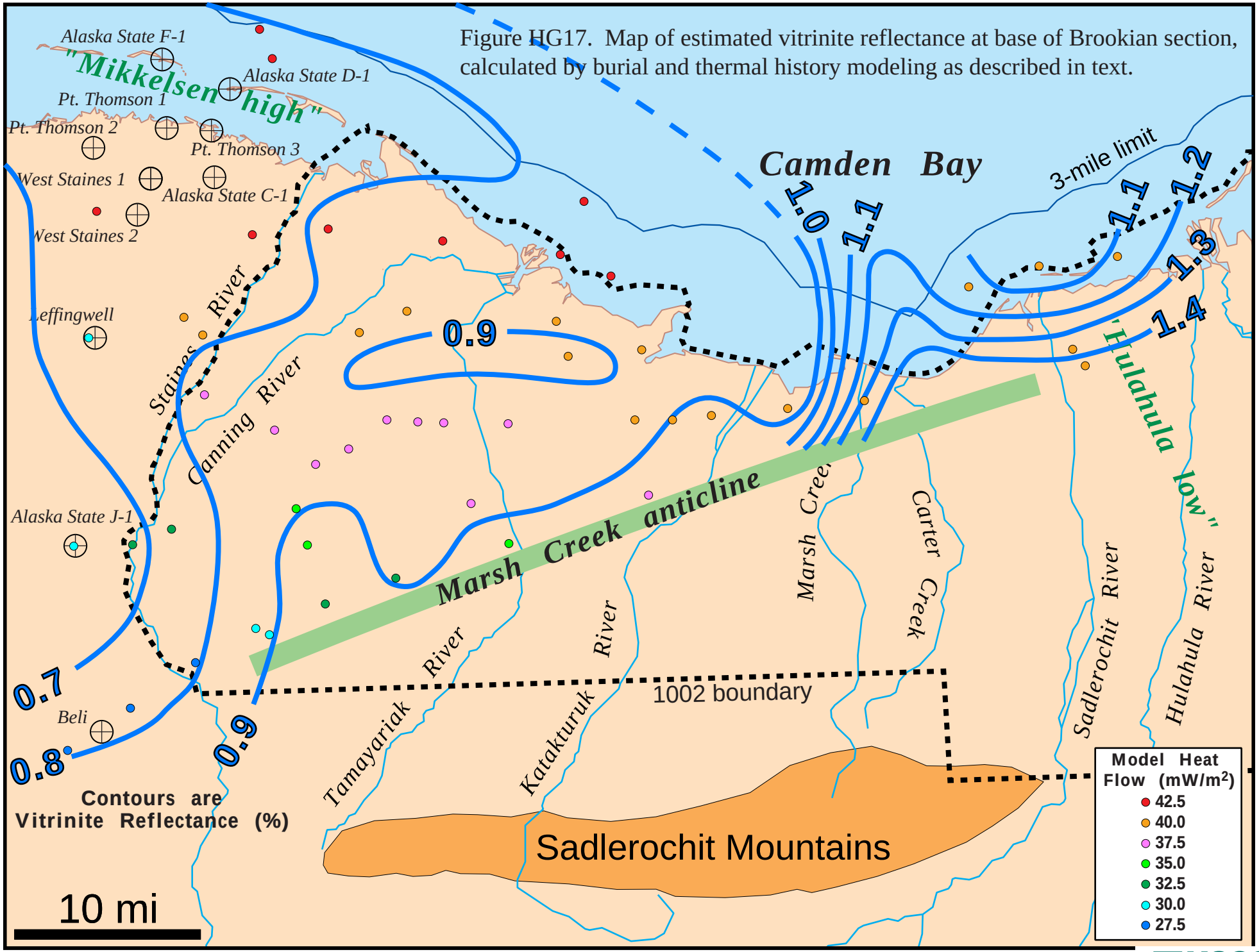

Figure HG18. Map of estimated transformation ratio at base of Brookian section, calculated by burial and thermal history modeling as described in text and assuming type II kerogen kinetics.

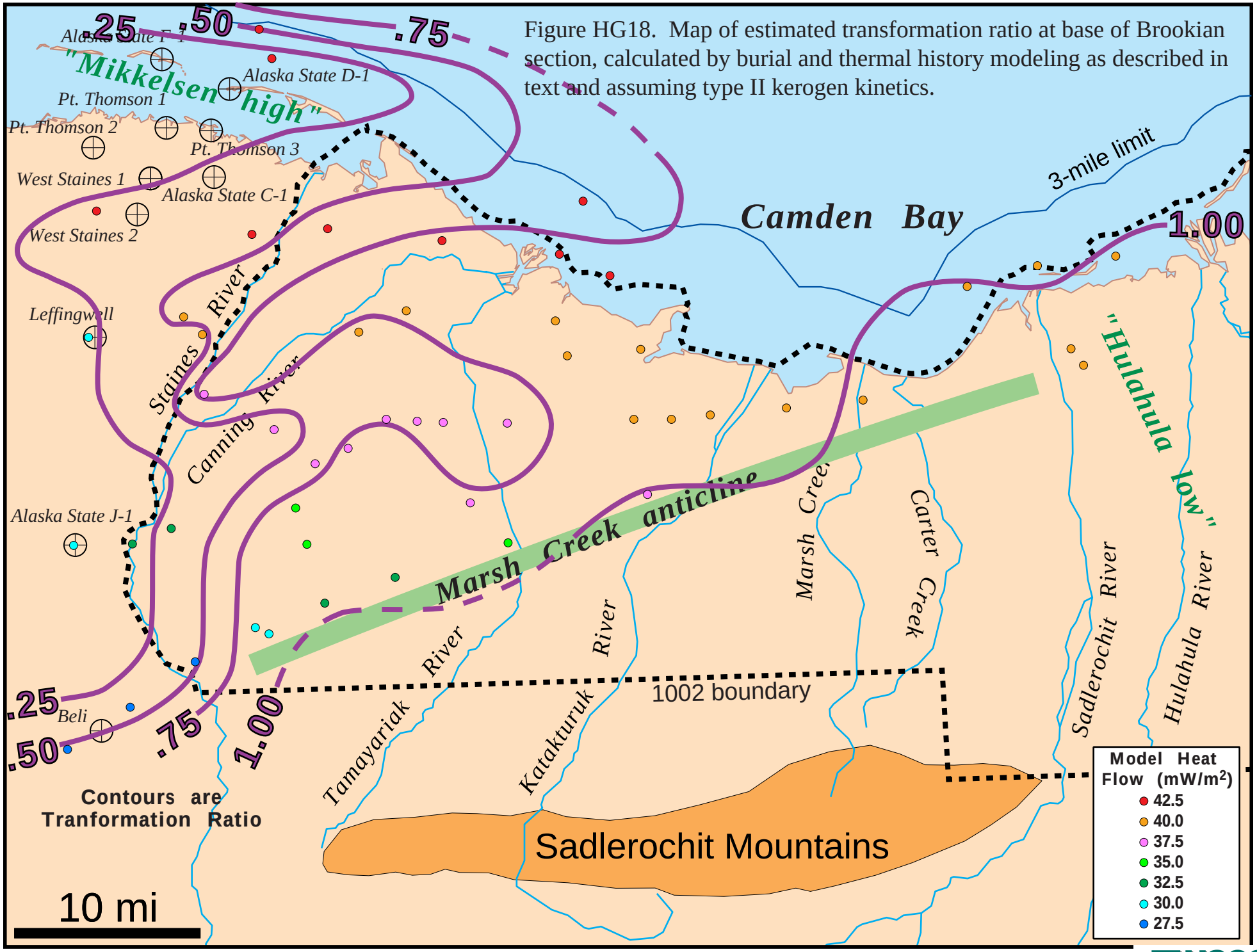

Figure HG19. Map of estimated age of onset of main phase of oil generation (transformation ratio = 0.25) at base of Brookian section, calculated by burial and thermal history modeling as described in text and assuming type II kerogen kinetics.

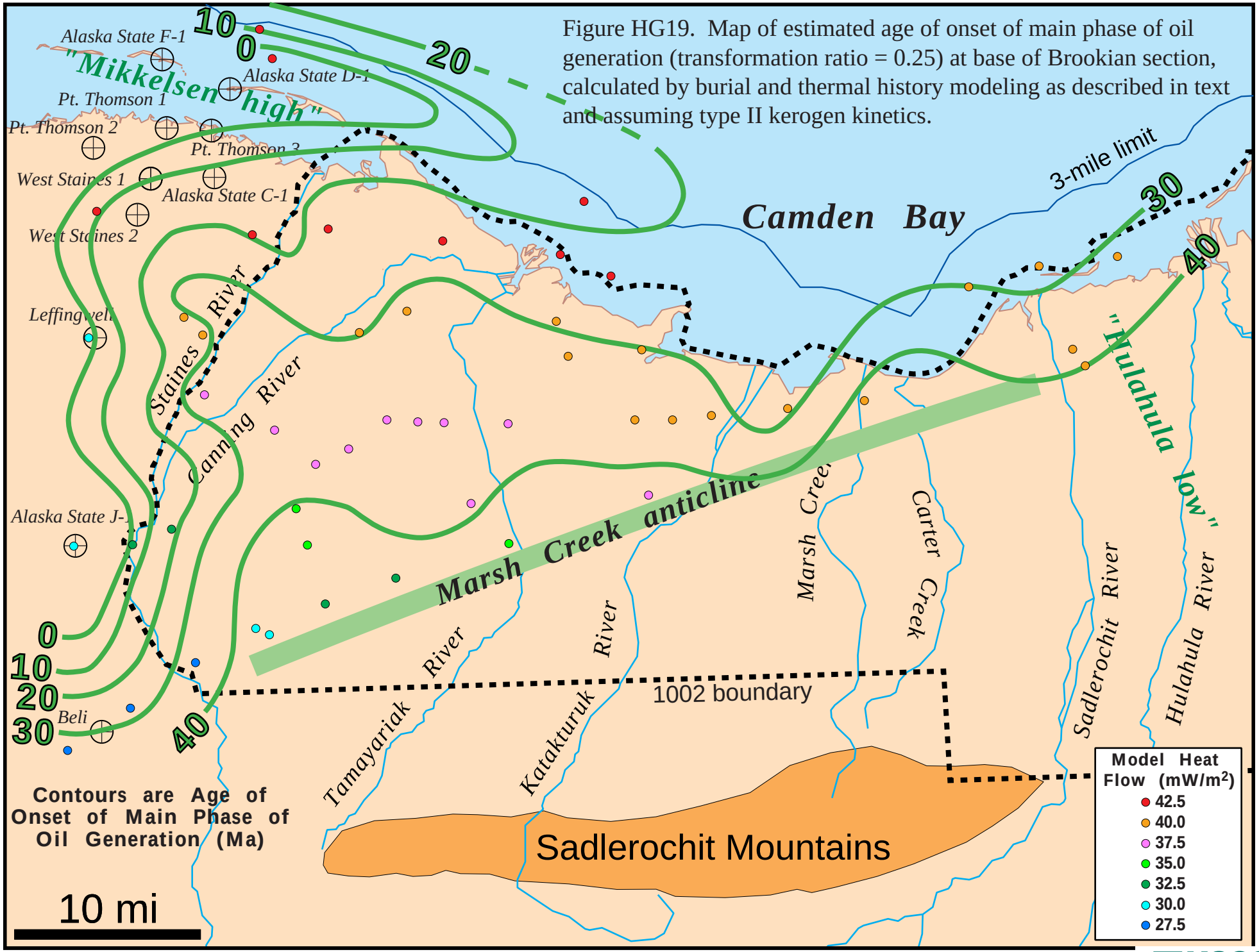

Figure HG20. Map of estimated age of end of main phase of oil generation (transformation ratio = 0.65) at base of Brookian section, calculated by burial and thermal history modeling as described in text and assuming type II kerogen kinetics.

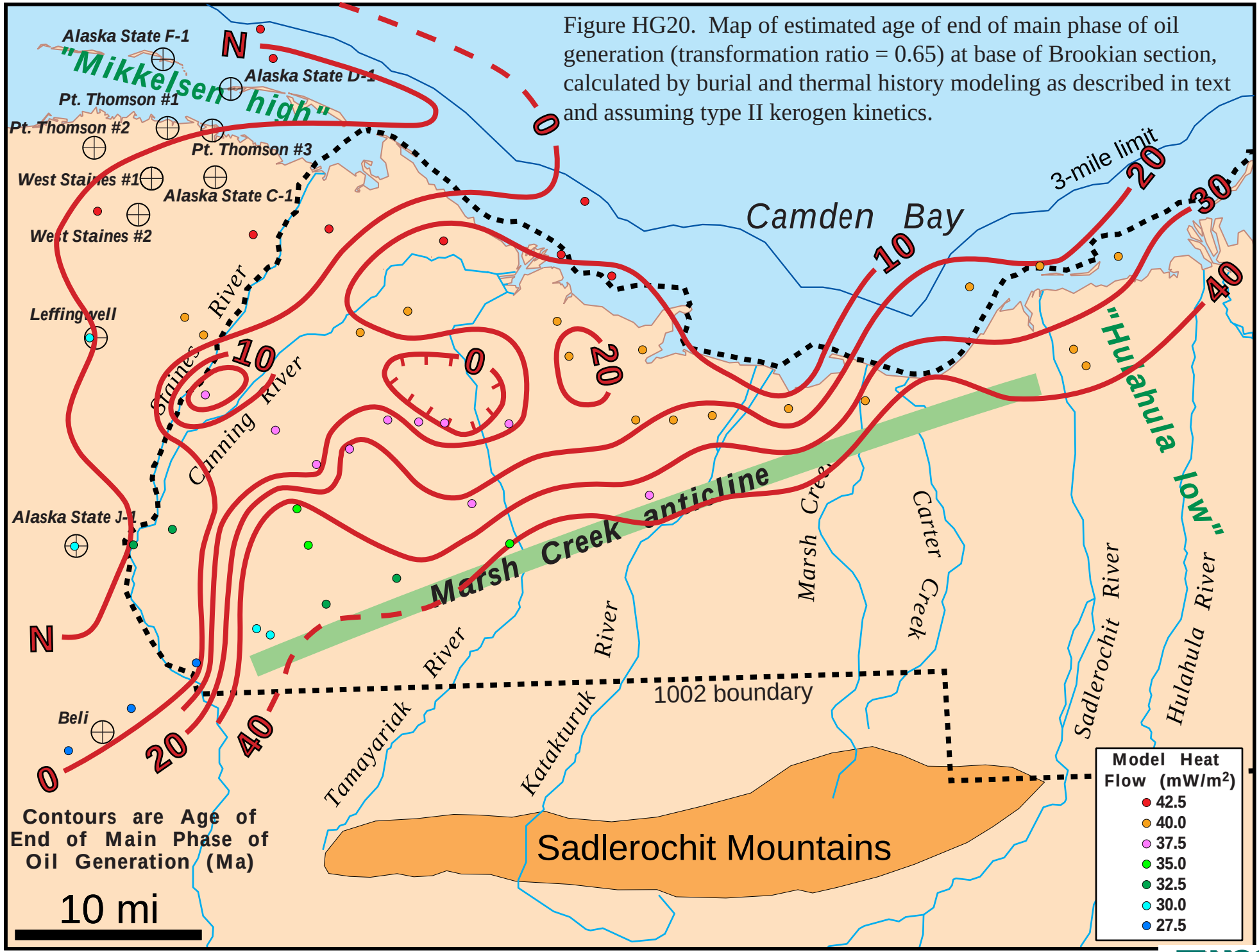

Table HG1. Estimates of present day heat flow for wells located west of the ANWR 1002 area based on bottom-hole temperatures. Approach 1 uses base of permafrost as datum (-1¡C temperature assumed) and approach 2 assumes ground surface as datum (-8.5¡C temperature assumed). Measured bottom hole temperatures are provided by Nelson and others (Chap. WL).

	Calculated Heat Flow (mW/m^2)	
Well	Approach 1	Approach 2
datum:	base permafrost	ground surface
Point Thomson Area		
Alaska State C-1	46	41
Point Thomson Unit 1	50	46
Point Thomson Unit 2	47	38
West Staines (18-9-23)	47	44
West Staines State 2	46	42
Composite (5 wells)	48	43
E De K Leffingwell	45	33
Alaska State J-1	55	37
Beli Unit 1	55	50